Bidirectional interaction between Protocadherin 8 and transcription factor Dbx1 regulates cerebral cortex development

Andrzej W Cwetsch[1,2,3], Javier Gilabert-Juan*[4], Sofia Ferreira*[1,2], Matthieu X. Moreau*[1,2], Yoann Saillour[1,2], Elodie Delberghe[1,2], Jose González Martínez[5], Ugo Borello[1,2], Frédéric Causeret[1,2] and Alessandra Pierani[1,2]

1- Université Paris Cité, Imagine Institute, Team Genetics and Development of the Cerebral Cortex, F-75015, Paris, France
2- Université Paris Cité, Institute of Psychiatry and Neuroscience of Paris, INSERM U1266, F75014, Paris, France
3 - Instituto de Biotecnologia y Biomedicina (BIOTECMED), Universidad de Valencia, Burjassot, Spain
4 - Departamento de Anatomía, Histología y Neurociencia, Universidad Autónoma de Madrid, Madrid, Spain
5 - Cell Division and Cancer group, Spanish National Cancer Research Centre (CNIO), Madrid, Spain.

Corresponding author: alessandra.pierani@inserm.fr
* Equal contribution

SUMMARY

Brain development requires correct tissue patterning and production of appropriate cell types. Transcription factors (TFs) play essential roles in these processes, regulating the expression of target genes responsible for neuronal subtypes specific features. Cell adhesion molecules are key components of neuronal identities that control cell sorting, migration, neurite outgrowth/guidance and synaptogenesis. To date, the link between TFs and cell adhesion molecules is considered to be unidirectional. Here, we demonstrate that ectopic expression of Dbx1 leads to spatio-temporally restricted increased expression of *Pcdh8* and cell aggregation, together with changes in neuronal identity. Surprisingly, Pcdh8 overexpression also induces Dbx1 expression as well as a complete reorganisation of apico-basal polarity and dorso-ventral patterning *via* Notch signalling. Altogether, our work therefore points to cell adhesion molecules as unexpected, yet important, players in the regulation of cell identity and, in particular, Pcdh8 through its bidirectional interaction with the Dbx1 transcription factor.

INTRODUCTION

Early steps of brain development rely on tightly controlled action of transcription factors (TFs) that organize the dorso-ventral (DV) axis of the central nervous system (CNS). The precise expression of TFs in domains along the DV axis ensures robust patterning and their faulty regulation leads to the disruption of the DV organisation and/or cell identity (Pierani *et al.*, 1999; Marklund *et al.*, 2010; Godbole *et al.*, 2017; Arai *et al.*, 2019; Leung *et al.*, 2022). Among other TFs, in the early mouse developing telencephalon, the Developing Brain Homeobox 1 (Dbx1) gene shows a very precise expression in the ventral pallium (VP) just above the pallial-subpallial boundary (PSB) and the septum (Bielle *et al.*, 2005). Interestingly, Dbx1 was shown to function as a potent DV patterning and cell-fate determinant in different regions of the CNS, such as the mouse spinal cord (Pierani et al., 2001), rhombencephalon (Bouvier et al., 2010), diencephalon (Sokolowski *et al.*, 2016) and telencephalon (Arai *et al.*, 2019). However, it remains unknown how Dbx1 influences cell fate at the molecular level (Leung *et al.*, 2022).

Protocadherins (Pcdhs) are cell adhesion molecules that belong to the cadherin superfamily, and in vertebrates are subdivided into two subgroups: clustered (cPcdhs) and non-clustered Pcdhs (ncPcdhs). Their expression is spatiotemporally regulated during development, and they are involved in multiple processes related to proper CNS formation. In particular, δ-Pcdhs (i.e. Pcdh8, Pcdh9 and Pcdh19), a subgroup of ncPcdhs, have been associated with dendrite and axon formation, morphology, migration and guidance (Yasuda *et al.*, 2007; Biswas *et al.*, 2010; Bruining *et al.*, 2015; Cooper *et al.*, 2015; Bassani *et al.*, 2018; Pancho *et al.*, 2020; Cwetsch *et al.*, 2022). Moreover, human mutations in some δ-Pcdhs are associated to several neurodevelopmental disorders, such as autism, schizophrenia and epilepsy (Kahr *et al.*, 2013). Recently, the expression of specific cell adhesion molecules has been shown to follow that of TFs in selected progenitor domains in response to sonic hedgehog (Shh), and suggested to be involved in the patterning robustness of the zebrafish spinal cord (Tsai *et al.*, 2019). Furthermore, it was shown that in the mammalian neocortex, patterned Pcdh expression biases fine spatial and functional organization of individual neocortical excitatory neurons (Lv *et al.*, 2022). However, a function in the regulation of TFs expression has not been addressed.

We previously demonstrated that at embryonic day 11.5 (E11.5), ectopic expression (EE) of Dbx1 (hereafter Dbx1 EE) in the dorsal pallium (DP) of the developing mouse brain imparts cell identity by inducing ectopic Cajal-Retzius (CRs) and subplate-like (SP) neuron fate (Arai *et al.*, 2019), thus resulting in changes in cell fate in the DP. The molecular mechanism behind this process, however, remains unknown. Here we report that Dbx1 EE leads to cell aggregation through Pcdh8 upregulation and that Pcdh8 is required for Dbx1-induced neuronal fate specification. We used single-cell RNA sequencing (scRNAseq) to characterize distinct expression dynamics for both genes during neuronal differentiation at the VP and septum. Consistently, we reveal that Pcdh8 EE induces a cell-autonomous upregulation of Dbx1 as well as non-cell-autonomous defects in cell proliferation and tissue patterning, resulting in a massive reorganization of the cortical primordium. Finally, we identify Notch signalling as a possible downstream effector of Pcdh8. Our findings therefore point to cell adhesion molecules, in particular Pcdh8, as players acting not only downstream, but also upstream of TFs during brain development.

RESULTS

Ectopic Dbx1 expression in the lateral pallium induces cell aggregation

Using *in utero* electroporation (IUE), we previously investigated the effects of ectopic pCAGGS-Dbx1-iresGFP expression in the E11.5 mouse DP. We found that Dbx1 EE induces the production of neurons harbouring features of Cajal-Retzius ($Reln^+/Calr^+$ (Calretinin/Calb2)) and subplate $Nr4a2^+$ (Nurr1) fates 48h after electroporation (Arai *et al.*, 2019). Surprisingly, when electroporation of Dbx1 at E11.5 encompassed lateral and ventral pallial domains, we noticed 48h later, that transfected cells tended to aggregate forming cohesive clusters (Figure 1A, B, Supplementary Figure 1A, C). Such clusters were preferentially formed in the lateral pallium (LP) (Figure 1C, D) at the border between the ventricular/subventricular zone (VZ/SVZ) and the cortical plate (CP) (Figure 1B, Supplementary Figure 1C. They were rarely observed in the dorsal or medial cortex, or in any region of GFP-electroporated control brains (Figure 1B, D). Aggregates also failed to form when IUE was performed one day later, at E12.5, suggesting a spatio-temporal modulation in the response to Dbx1 EE (Supplementary

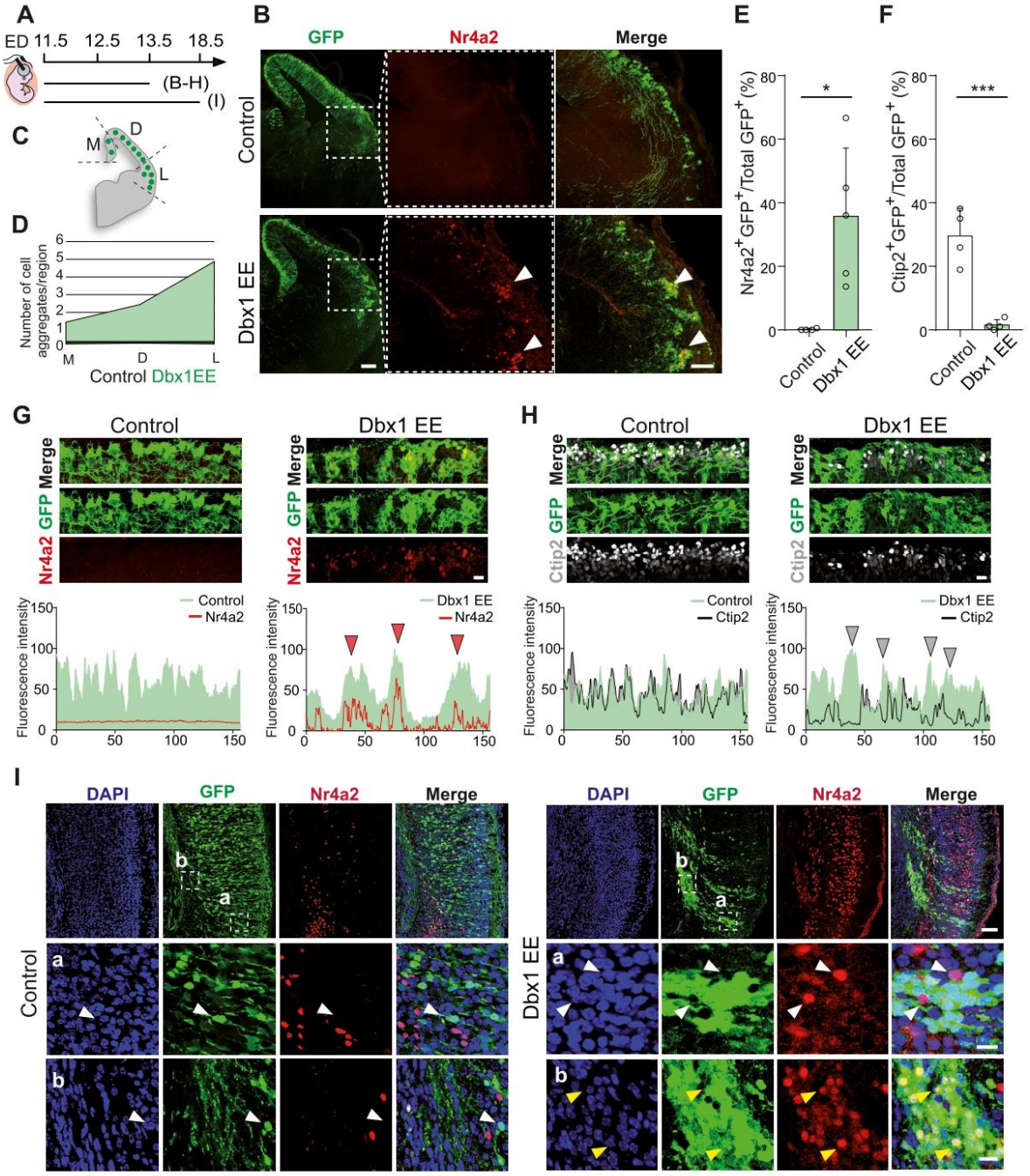

Figure 1. Dbx1EE induces cell aggregation in lateral pallium

(A) Schematic timeline of the IUE. **(B)** Confocal images of GFP (green) fluorescence in coronal sections of E13.5 mouse brain cortices electroporated at E11.5 with a control GFP vector or Dbx1 EE co-labeled with Nr4a2 (red). Higher magnification of the dashed squares is shown on the right, with Nr4a2 and GFP labeling. White arrowheads indicate aggregates. Scale bars: 200 µm (left) and 100 µm (right). **(C)** Scheme of aggregate analysis in M-medial, D-dorsal, L-lateral pallium. **(D)** Aggregates formation analysis from control (n=6) and Dbx1 EE (n=6) brain sections as showed in (C). **(E, F)** Percentages of $Nr4a2^{+}GFP^{+}$ (E) and $Ctip2^{+}GFP^{+}$ (F) cells over the total of GFP^{+} cells. Data are mean ± SEM; circles indicate values from single animals (n=5 (E); n=4 (F)); Student's t-test, *p=0.01 (E), ***p=0.0008 (F). **(G, H)** Top: representative confocal images of E13.5 mouse coronal sections showing GFP^{+} (green) cells electroporated with a control vector or Dbx1 EE co-labeled for Nr4a2 (red) (G) or Ctip2 (gray) (H). Scale bar: 25 µm. Bottom: fluorescent intensities of GFP^{+} (green area) cells (control vector or Dbx1 EE) and $Nr4a2^{+}$ (red line, G) or $Ctip2^{+}$ (gray line, H), along the cortical surface expressed in µm. Red (G) or gray (H) arrowheads show positive (Dbx1 EE GFP^{+} areas and Nr4a2 labeling) or negative (Dbx1 EE GFP^{+}

areas and Ctip2 labeling) fluorescent intensity correlation. **(I)** Top: confocal images of GFP$^+$ (green) fluorescence in coronal sections of E18.5 mouse brain cortices after IUE at E11.5 with a control vector or Dbx1 EE co-labeled with Nr4a2 (red), DAPI (blue) counterstaining. Higher magnification of the dashed squares (a) and (b) is shown in the bottom panels. White arrowheads point to Nr4a2$^+$ cells present in the electroporated area while yellow arrowheads point to Dbx1 EE/ Nr4a2$^+$ cells. Scale bars: top panel 200 µm, bottom panel 25 µm.

Figure 1A, B). In line with our previous findings, we found numerous SP-like cells expressing Nr4a2 within the Dbx1-induced aggregates, but not in control GFP-electroporated cells (Figure 1B, E, G, Supplementary Figure 1E). Conversely, cells expressing Ctip2, a marker of early generated neurons, were never observed within the clusters and appeared excluded from the GFP$^+$ regions (Figure 1F, H, Supplementary Figure 1E). Indeed, when we measured immunofluorescence (IF) intensity of Nr4a2$^+$ or Ctip2$^+$ neurons aligned with the GFP intensity signal of Dbx1 EE cells, we observed a positive and negative correlation, respectively (Figure 1G, H). Surprisingly, Dbx1-induced aggregates were Reln$^-$ and Calb2$^-$ with some Reln$^+$ and Calb2$^+$ individual cells at the cortical surface (Supplementary Figure 1F, G). All electroporated GFP$^+$ cells were expressing Dbx1 (Figure Supplementary 1D). When embryos were collected 7 days after IUE (E11.5-18.5), we observed accumulation of the Dbx1 EE/ Nr4a2$^+$ cells in the intermediate zone (IZ)/SP and Dbx1 EE$^-$/Nr4a2$^+$ within the CP (Figure 1I).

Altogether, these results show that Dbx1 EE not only affects neuronal fate specification with CRs at the surface and SP-like deeper, but also promotes cell-cell adhesion in a cell-autonomous (CA) manner. In addition, we found that Dbx1-induced cell aggregation is spatio-temporally restricted by the competence of the cortical neuroepithelium.

Pcdh8 and Dbx1 show sequential or concomitant expression respectively in the VP or septum

To begin investigating the molecular mechanisms behind Dbx1-induced aggregation, we took advantage of previously published bulk transcriptomic profiles of fluorescence-activated cell sorting (FACS)-purified Dbx1-derived cells collected from dorsomedial and dorsolateral cortices of E12.5 *Dbx1^{Cre}; Rosa26^{YFP}* embryos (Figure 2A, B, C) (Griveau *et al.*, 2010). We compared the expression level of genes belonging to the Protocadherin (Figure 2B) and Cadherin (Figure 2C) families, two major players in neuronal adhesion (Halbleib and Nelson, 2006; Suzuki and Takeichi, 2008; Peek *et al.*, 2017). We found that *Cdh2* (also known as *Ncad*), *Pcdh8*, *Pcdh9* and *Pcdh19* stood out with ~10-fold higher expression levels in comparison to other adhesion molecules (Figure 2B, C). To better appreciate the possible implication of such candidates downstream of Dbx1 we used scRNAseq. We first used a previously generated dataset sampling cell diversity around the pallial-subpallial boundary (PSB) at E12.5 (Moreau et al., 2021). We found *Cdh2*, *Pcdh9* and *Pcdh19* broadly expressed, with no specific enrichment (https://apps.institutimagine.org/mouse_pallium/). In contrast, *Pcdh8* displayed an interesting expression pattern, especially in apical progenitors (APs) in sub-pallial territories and in the VP, but not in lateral and dorsal pallial regions (Figure 2D). Since Dbx1 expression is initiated in APs of the VP but strongly increases upon transition to the basal progenitor (BP) state, we compared the temporal dynamics of both genes. We used a previously reconstructed differentiation trajectory in which cells of the VP lineage are aligned along a pseudotime axis corresponding to their differentiation state, from AP to neuron (Moreau et al. 2021). We found that *Pcdh8* and *Dbx1* are expressed sequentially in the VP lineage, with *Pcdh8* peaking in APs, followed by *Dbx1* in BPs (Figure 2E). Next, to investigate *Pcdh8* expression in other Dbx1-derived cell lineages, we performed scRNAseq on dissected septum explants collected from

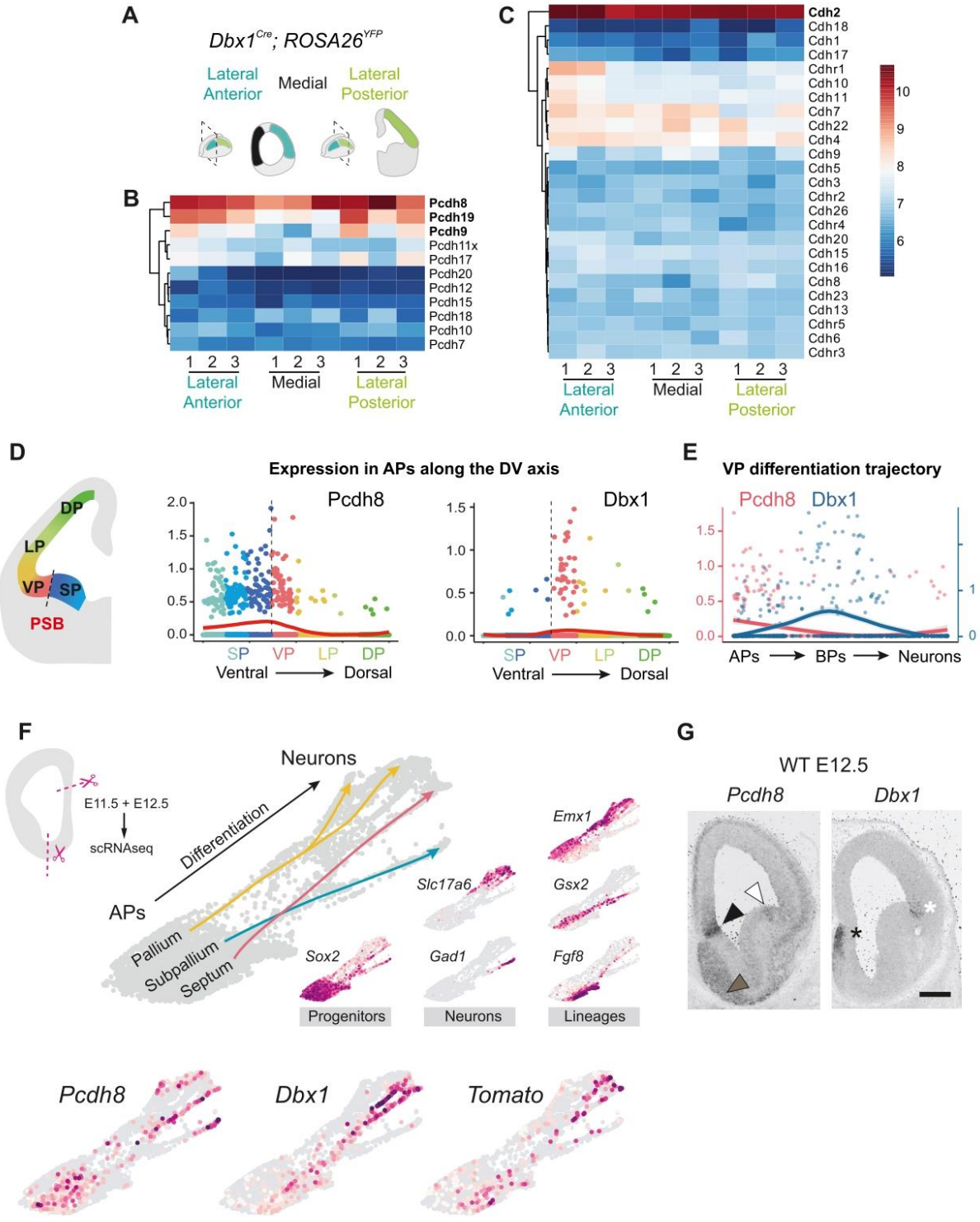

Figure 2. The endogenous expression of Pcdh8 and Dbx1 partially overlaps

(A) Experimental design: E12.5 *Dbx1*^{Cre};*Rosa*^{26YFP} brain with marked dissected regions of lateral anterior, lateral posterior and medial areas for bulk transcription profiling upon FACS-sorting of YFP^{+} cells (B,C). **(B)** Heat map of microarray analysis of E12.5 *Dbx1*^{Cre};*Rosa*^{26YFP} brains for protocadherins (Pcdhs). **(C)** Heat map of microarray analysis of E12.5 *Dbx1*^{Cre};*Rosa*^{26YFP} brain for cadherins (Cdhs). Color scale (right) indicates the expression levels from low (blue) to high (red). **(D)** Comparison of gene expression trends of *Pcdh8* and *Dbx1* along pseudo dorso-ventral (DV) scores. Each dot represents one single apical progenitor (AP) color-coded according to the domain it belongs to (SP, subpallium; VP, ventral pallium; LP, lateral pallium; DP, dorsal pallium; PSB, pallial-subpallial

boundary). The red curve indicates the smoothed expression profile. **(E)** Comparison of *Pcdh8* and *Dbx1* gene expression trends along pseudotime in the *Pcdh8* (red) or *Dbx1* (blue) trajectory. **(F)** Left side: scheme of dissection for scRNAseq profiling. Septum SPRING representation of the dataset illustrating expression level of selected genes in marked differentiation trajectories compared to *Pcdh8* and *Dbx1* transcripts as well as *Tomato*. **(G)** Bright-field images of *in situ* hybridization for *Pcdh8* and *Dbx1* performed on E12.5 WT coronal sections. White, black and brown arrow points to *Pcdh8* expression on the ventral side of the PSB, on the Septum VZ and postmitotic stream of cells, respectively. White and black star mark the Dbx1 expression in the VP dorsal to the PSB and Septum, respectively. Scale bar: 100µm.

E11.5 and E12.5 embryos, the latter being derived from $Dbx1^{Cre};Rosa^{Tomato}$ animals to allow genetic tracing (Figure 2F). After quality control, we obtained a dataset of 5299 cells containing progenitors of the septum ($Fgf8^{+}$), and neighbouring pallial ($Emx1^{+}$) and sub-pallial ($Gsx2^{+}$) domains, from which stemmed excitatory ($Slc17a6^{+}$) and inhibitory (*Gad1*) neuronal lineages (Figure 2F; Supplementary Figure 2A, B). As for the PSB, *Pcdh8* displayed the most interesting pattern compared to that of *Dbx1* (https://apps.institutimagine.org/mouse_septum/). Thus, robust co-expression of *Dbx1* and *Pcdh8* was observed in septal-derived postmitotic excitatory neurons ($Tbr1^{-}/Slc17a6^{+}$) characterized by the expression of transcription factors *Isl1, Onecut2* and *Onecut3* (Figure 2F; Supplementary Figure 2A, B). We validated these findings by *in situ* hybridization (ISH). At E12.5 we observed strong *Pcdh8* mRNA enrichment in progenitor domains adjacent to the most characteristic telencephalic regions of *Dbx1* expression, the VP dorsal to the PSB and the septum (Bielle et al. 2005) (Figure 2G). However, lower *Pcdh8* expression was also detected in pallial neurons and overlapping with *Dbx1* expression at the VP (Figure 2G). The pattern of *Pcdh8* expression was conserved at the earlier stage E11.5 (Supplementary Figure 3A). Pcdh8 expression in the VP and in Dbx1-derived neurons was further confirmed by co-immunostaining of βgal and anti-Pcdh8 (antibody validation at E12.5, Supplementary Figure 3B) on brain sections of E11.5 and E12.5 $Dbx1^{LacZ/+}$ embryos (Supplementary Figure 3C, D).

We therefore conclude that *Dbx1* and *Pcdh8* display interrelated expression patterns in the developing telencephalon, occurring either consecutively during neuronal differentiation at the VP or concomitantly in the septal lineage.

Dbx1 EE induces Pcdh8 expression

To address whether Dbx1 EE influences the expression of *Pcdh8* we performed quantitative reverse transcription polymerase chain reaction (RT-qPCR) on lateral cortical tissue dissected 48h after Dbx1-iresGFP IUE or a GFP control expression vector (E11.5-13.5) (Figure 3A, B). We included *Reln, Calb2* and *Nr4a2* in the analysis given their known upregulation upon Dbx1 EE in the dorsal cortex (Arai *et al.*, 2019), also *Ctip2* given its exclusion from Dbx1-induced aggregates (Figure 1F, H), and *Pcdh9, Pcdh19* and *Ncad*. As expected, we found increased levels of *Dbx1* mRNA in Dbx1-electroporated regions compared to controls (Figure 3C). The expression levels of *Pcdh8*, *Nr4a2* and *Calb2* transcripts were significantly increased in the electroporated areas, but no changes were observed for the remaining analysed genes (Figure 3D). Similar results were obtained just 24h after IUE (E11.5-12.5), with a significant upregulation of *Dbx1*, *Pcdh8* and *Nr4a2* transcripts, arguing for a rapid, if not direct, regulatory effect (Figure 3E, F). Additionally, following Dbx1 IUE (E11.5-13.5), we observed a significant negative correlation between *Dbx1* and *Pcdh19* gene expression (Supplementary Figure 4A), which was not the case for other tested cadherins (i.e. *Pcdh8*, *Pcdh9* and *Ncad*) (Supplementary Figure 4A), pointing to other possible partners in gene co-regulation networks. By contrast, Dbx1 IUE at E12.5 (E12.5-14.5) did not alter *Pcdh8* and *Nr4a2* expression, but resulted in the upregulation of *Pcdh9*, *Pcdh19*, *Ncad*, and *Ctip2* (Supplementary

Figure 4B, C, D, E), which overall aligns with the absence of cell aggregates upon Dbx1 EE at this developmental stage (Supplementary Figure 4F). These results thus reflect the important changes that occur in the ability of the cortical neuroepithelium to respond to Dbx1 between E11.5 and E12.5. Furthermore, these point to possible distinct Pcdhs and Cadhs programs induced by Dbx1 at these stages.

In order to validate these findings, and determine whether changes in gene expression are cell-autonomous (CA), we performed immunostaining of Pcdh8 and Dbx1 on E11.5 Dbx1-electroporated brain sections. We confirmed higher CA Pcdh8 protein expression in Dbx1 EE cells at E13.5 (Figure 3G). At E18.5, the picture was more complex as we observed both clusters of Pcdh8^{high} Ctip2^{-} Nr4a2^{+} cells below the CP, and Pcdh8^{low} Ctip2^{+} Nr4a2^{-} cell streams within the CP (Supplementary Figure 5A). Furthermore, we found that, following IUE at E11.5, the regular lateral Pcdh19 protein expression at E13.5 on control sections was strongly reduced specifically where Dbx1-induced aggregates were formed (Supplementary Figure 5B), consistently with *Pcdh19* gene expression showing a negative correlation with that of *Dbx1* in the RT-qPCR data (Supplementary Figure 4A) and thus with *Dbx1* repressing *Pcdh19* transcription.

Overall, these findings indicate a rapid and possibly time-restricted action of Dbx1 EE on *Pcdh8* upregulation as well as *Pcdh19* repression in a CA manner.

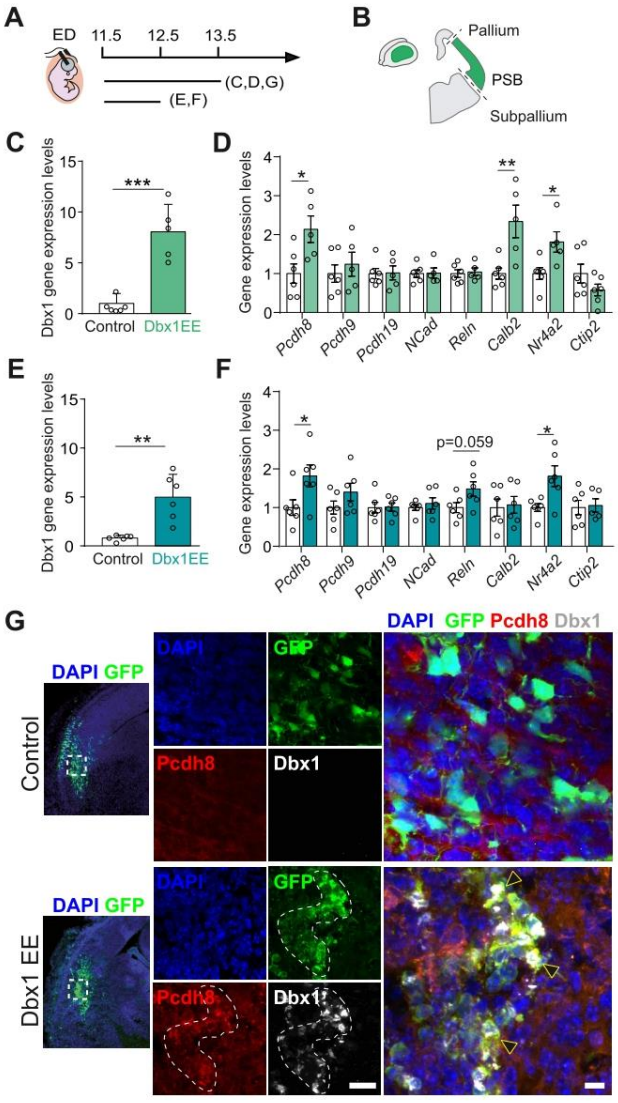

Figure 3. Dbx1 EE induces Pcdh8 gene expression in the electroporated area

(A) Schematic timeline of the IUE. **(B)** Electroporated region dissection scheme. **(C-F)** qPCR quantifications of *Dbx1* (C, E) or *Pcdh8*, *Pcdh9*, *Pcdh19*, *Ncad*, *Reln*, *Calb2*, *Nr4a2* and *Ctip2* (D, F) gene expression upon IUE of a control vector or Dbx1 EE at E11.5 and analysis at E13.5 (C, D) and E12.5 (E, F). Data are mean ± SEM; circles indicate values from single electroporated samples (n=6 controls, n=5-6 Dbx1 EE). Student's t-test: ***p=0.0002 (C), **p=0.0014 (E), *$p\leq0.05$ and **$p\leq0.01$ (D, F). **(G)** Confocal images of GFP^{+} (green) fluorescence in coronal sections of E13.5 mouse brains after IUE at E11.5 with a control vector or Dbx1 EE co-labeled with Pcdh8 (red) and Dbx1 (gray), with DAPI (blue) counterstaining. Dashed areas show high Pcdh8 expression. Black arrowheads indicate cells exhibiting Dbx1 and Pcdh8 colocalization. Scale bar: 100 µm.

Pcdh8 is required for Dbx1-induced adhesion and fate specification

Next, to determine the contribution of Pcdh8 in Dbx1-induced cell aggregation, we investigated the epistasis between Dbx1 and Pcdh8 by combining Dbx1 EE and *Pcdh8* knock-down (KD). We first designed three shRNA constructs targeting *Pcdh8* and

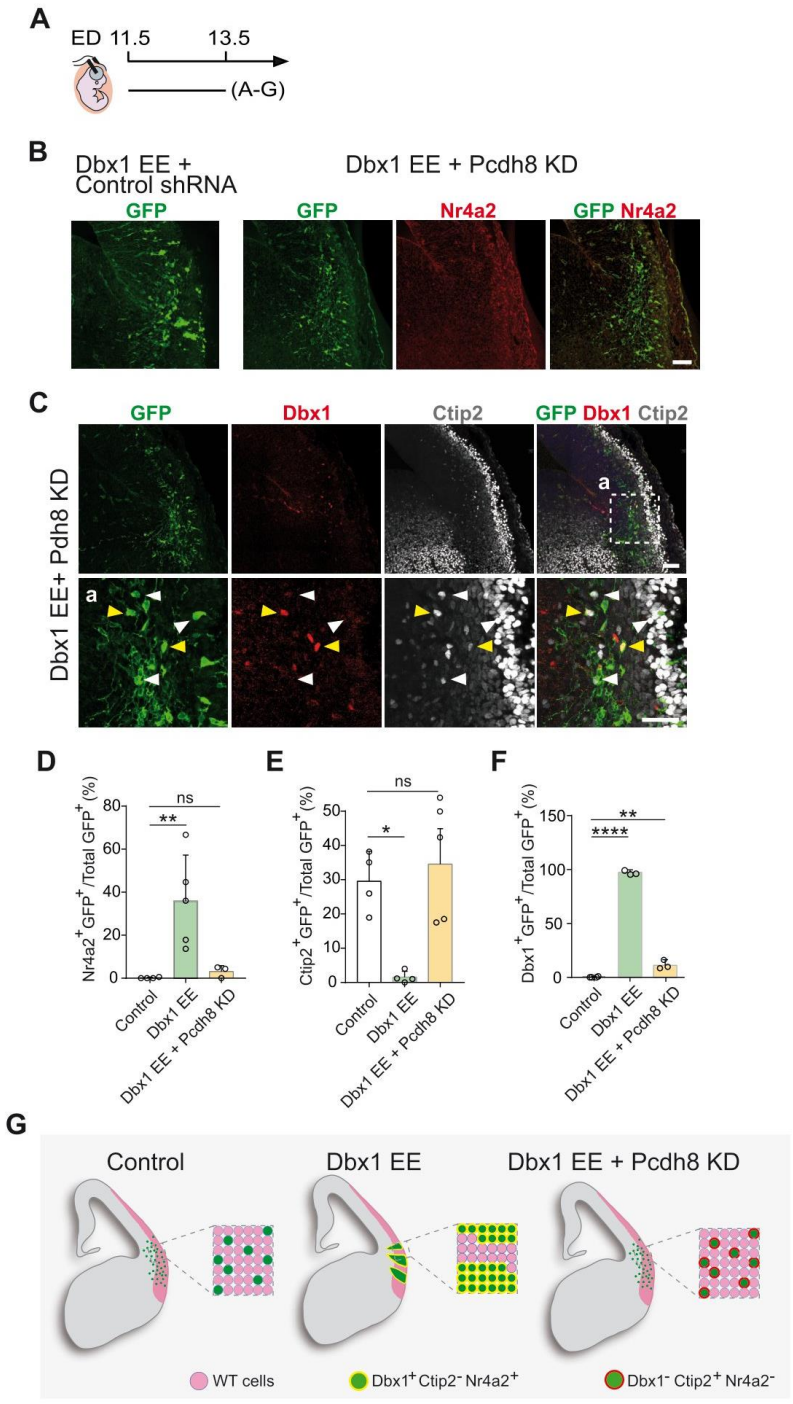

Figure 4. Pcdh8 is responsible for the Dbx1 EE phenotype

(A) Schematic timeline of the IUE. **(B-C)** Confocal images of GFP$^+$ (green) fluorescence in coronal sections of E13.5 mouse brains after IUE at E11.5 with Dbx1 EE + control shRNA (SCR) or Dbx1 EE + Pcdh8 KD co-labeled with Nr4a2 (red) (B), or with Dbx1 (red) and Ctip2 (gray) (C). Higher magnification of the dashed square (a) in (C) is shown in bottom panels. White and yellow arrowheads point to Dbx1$^-$ and Dbx1$^+$ cells, respectively. Scale bars 100 µm. **(D-F)** Percentages of Nr4a2$^+$GFP$^+$ (C), Ctip2$^+$GFP$^+$ (D) and Dbx1$^+$GFP$^+$ (E) cells over the total of GFP$^+$ cells. Data are mean ± SEM; circles indicate values from single animals (n=3-4 controls, n=3-5 Dbx1EE (Dbx1 EE + control shRNA), n=3-5 Dbx1 EE + Pcdh8 KD. One-way ANOVA, *post hoc* Holm-Sidak: ns, not significant, **p=0.0099 (D), *p<0.05 (E), ****p<0.0001 and **p=0.0021 (F). **(G)** Scheme of Pcdh8 KD effect on Dbx1 EE-induced aggregate formation phenotype and cell fate.

determined their efficiency by western blot analysis 48h after co-transfecting with a *Pcdh8* expression vector into HEK293T cells. We selected the most effective shRNA, which downregulated *Pcdh8* expression by 51% compared to a control shRNA (Supplementary Figure 6A). When electroporated alone, the Pcdh8 shRNA construct did not induce obvious changes in cell identity (Nr4a2, Ctip2) or cell aggregation (Supplementary Figure 6B, C, D). Next, we co-electroporated E11.5 mouse brains with Dbx1 EE and Pcdh8 shRNA or control shRNA constructs (Figure 4A, B, C). Interestingly, we observed no aggregate formation (Figure 4B, C), thus indicating that Pcdh8 is required for Dbx1-induced cell adhesion. Moreover, we observed a reduced number of GFP^+Nr4a2^+ cells (Figure 4D), and an increased number of GFP^+Ctip2^+ cells (Figure 4E) compared to Dbx1 EE alone, indicating that Pcdh8 is also required for Dbx1-induced fate determination. Since Pcdh8 KD rescued the phenotypes induced by Dbx1 EE, we decided to monitor Dbx1 expression upon Pcdh8 KD. Surprisingly, we observed numerous $GFP^+/Dbx1^-$ cells (Figure 4C, F, G) in comparison to Dbx1 EE alone (Figure 3G, Supplementary Figure 1C, D). Since Dbx1 EE is driven by a plasmid bearing a heterologous CAG promoter, the effect of Pcdh8 shRNA on Dbx1 protein expression is likely post-transcriptional.

We thus conclude that Pcdh8 is an essential component in Dbx1-induced aggregation as well as cell-fate determination.

Pcdh8 overexpression results in major reorganization of pallial domains

To further investigate epistasis between Dbx1 and Pcdh8, we performed Pcdh8 EE in the LP, which is a territory devoid of Dbx1 expression, by IUE at E11.5 (E11.5-13.5) using a pCAGGS-Pcdh8-iresGFP plasmid. We observed that the Pcdh8 gain-of-function (from now on called for simplification Pcdh8 EE) (Supplementary Figure 6A, E) resulted in cortical plate thickening compared to the contralateral untransfected side of the same brain section (Figure 5A, B, C). ISH experiments revealed major tissue reorganization, consisting in the formation of large circumferential GFP^+ structures that recapitulated the DV partitioning of pallial domains with patches or stripes of cells expressing the ventral markers *Shh* or *Gsx2* segregated from cells positive for the dorsal markers *Lhx2* or *Bhlhe22* (coding Bhlhb5) (Figure 5D). Moreover, we observed that, markers of cycling progenitors such as Pax6 (Figure 5E, F) or *Notch1* (Figure 5D) were affected and extended outside of the VZ. Strikingly, *Dbx1*, which is normally restricted mostly to BPs of the VP, was found expressed throughout the electroporated area (Figure 5D). Altogether, Pcdh8 EE caused the local overgrowth of rosette-like structures characterized by Pcdh8, *Dbx1*, *Bhlhbe22* and *Shh* expressing cells in the outer layer segregating and organising *Pax6*, *Lhx2* and *Notch1* cells in the centre. These rosettes often displayed a central lumen lined by $PH3^+$ mitotic cells surrounded by GFP^+ ($Pcdh8^+$) cells (Figure 5G, H) and delimited by $Ncad^+$ apical junctions (Figure 5I).

We therefore conclude that modulation of cell adhesion through Pcdh8 expression disrupts the normal DV and apico-basal polarity of the telencephalic neuroepithelium.

Cell-autonomous control of cell fate by Pcdh8

The very precise segregation of gene expression in outer and central domains of the observed rosette-like structures prompted us to evaluate more precisely the CA *versus* cell-non autonomous (CNA) function of Pcdh8. We initially performed Dbx1 IF on brain sections of E11.5-electroporated embryos, 48h after IUE (E11.5-E13.5), to find an almost complete colocalization, with 90% ± 5% of Pcdh8 EE

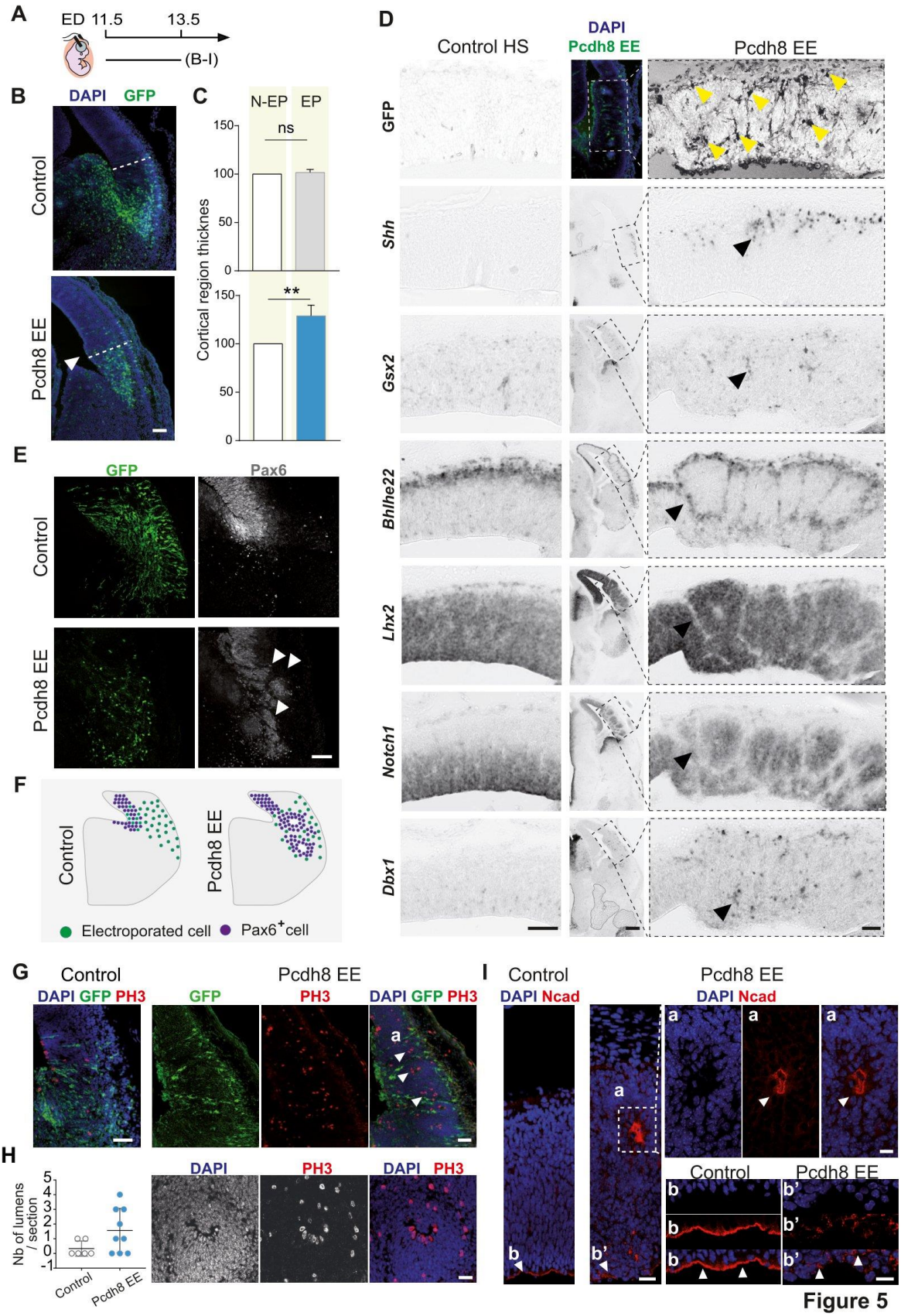

Figure 5. Pcdh8 overexpression causes reorganization of the developing pallium

(A) Schematic timeline of the IUE. **(B)** Confocal images of GFP$^+$ (green) fluorescence in coronal sections of E13.5 mouse brains after IUE at E11.5 with a control vector or Pcdh8 EE with DAPI (blue) counterstaining. White arrowhead points to the developing pallium overgrowth region. Dashed lines indicate the thickness measurement place. Scale bar: 200 µm. **(C)** Quantification of the cortical wall thickness as shown in (B) in control vector (top) or Pcdh8 EE (bottom) IUE normalized to the thickness of the control hemisphere. Data are mean ± SEM (n=4 animals/condition). Student's t-test: **p=0.0020, ns, not significant; N-EP, non-electroporated; EP, electroporated. **(D)** Confocal image of Pcdh8 EE (green) electroporated area (top middle panel), counterstained with DAPI (blue), and bright-field images of *in situ* hybridization for *Shh, Gsx2, Bhlhe22, Lhx2, Notch1* and *Dbx1* performed on 13.5 mouse brain sections after IUE at E11.5. Left panel represents control contralateral hemisphere from the same section as Pcdh8 EE (right panel). Higher magnification of the dashed rectangles in the middle panel of Pcdh8 EE is shown on the right. Yellow arrowheads point to cells displaying Pcdh8 EE. Black arrowheads point to altered mRNA expression. Scale bars: 200 µm (low magnification), 100 µm (high magnification). **(E)** Confocal images of GFP$^+$ (green) fluorescence in coronal sections of E13.5 mouse brains after IUE at E11.5 with a control vector or Pcdh8 EE co-labeled with Pax6 (gray). White arrowheads indicate the disorganization of Pax6$^+$ within the ventricular zone (VZ) and ventral pallium (VP). Scale bar: 100 µm. **(F)** Scheme of Pax6$^+$ cells distribution 48h after IUE as in (E). **(G)** Confocal images of GFP$^+$ (green) fluorescence in coronal sections of E13.5 mouse brains after IUE at E11.5 with a control vector or Pcdh8 EE co-labeled with PH3 (red) and DAPI (blue) counterstaining. White arrowheads indicate PH3$^+$ cells outside the VZ. Scale bar: 100 µm. Higher magnification of the indicated rosette (a) is shown on the bottom. Scale bar: 50 µm. **(H)** Quantification of the rosettes in control and Pcdh8 EE IUE brain sections. Data are mean ± SEM; circles indicate values of single sections (n=6 control, n=9 Pcdh8 EE). **(I)** Confocal images of representative regions of the control and Pcdh8 EE IUE (E11.5-E13.5) labeled with Ncad (red) and DAPI (blue) counterstaining. Higher magnification of the dashed square (a) is shown in the top right, and of the indicated VZ (b) and (b') in the bottom right. White arrowheads indicate disturbance of Ncad expression. Scale bars: 100 µm (left panel), 50 µm (a, b').

cells (GFP$^+$) being Dbx1$^+$ *versus* 0% of control GFP-transfected cells (Figure 6A, B, C). Furthermore, we observed that 31.5% ± 9.2% of Pcdh8 EE cells also expressed Nr4a2, compared to 0.1% in controls (Figure 6D, E). Similarly, we also observed an increase of Ctip2$^+$ and Bhlhb5$^+$ cells among Pcdh8-transfected cells, with 62.6 ± 8.1% compared to controls 33.4 ± 6.3% and 42.3 ± 15.9% compared to 16.7% ± 11.8% in controls respectively (Supplementary Figure 7A-E), confirming that Pcdh8 expression can control cell fate in a CA manner.

Given the massive disruption of the mitotic/postmitotic compartmentalization upon Pcdh8 EE (Figure 5D-H), we examined the expression of Notch ligands Delta1 and Jag1 (Stump *et al.*, 2002; Lasky and Wu, 2005) 48h following Pcdh8 IUE of E11.5 mouse brains (E11.5-E13.5) (Figure 7A). We found that a CNA Delta1 upregulation at the centre of Pcdh8-induced rosettes (Figure 7B) is accompanied by a CA decrease in Jag1 expression (Figure 7C), supporting the hypothesis that the Notch pathway is involved in the response to Pcdh8 EE and, thus, in changing the fate program of transfected progenitors (Figure 7D) and organization of the neuroephitelium (Figure 7E). To further investigate the mechanisms by which Pcdh8 controls the establishment of neuronal identity, we monitor cell proliferation and cell cycle exit following Pcdh8 IUE. We first quantified the number of mitotic progenitors among transfected cells (GFP$^+$PH3$^+$) and compared their positioning within the neuroepithelium of Pcdh8- and GFP-electroporated brains. We observed a complete CA switch from ventricular to abventricular mitotic figures upon Pcdh8 EE (Figure 7F, G, H, I), consistent with the observed disruption of apico-basal polarity (Figure 5D, G, I). Additionally, after the administration of a single pulse of EdU at E12.5, thus 24h post-surgery, quantification of EdU$^+$ transfected cells revealed that Pcdh8 EE led to a ~50% reduction in S-phase entry compared to controls (Figure 7A, F, J).

Taken together, these results show that manipulating cell adhesion through Pcdh8 overexpression is sufficient to affect neuronal fate acquisition in a CA manner *via* Notch signalling alteration and premature cell cycle exit.

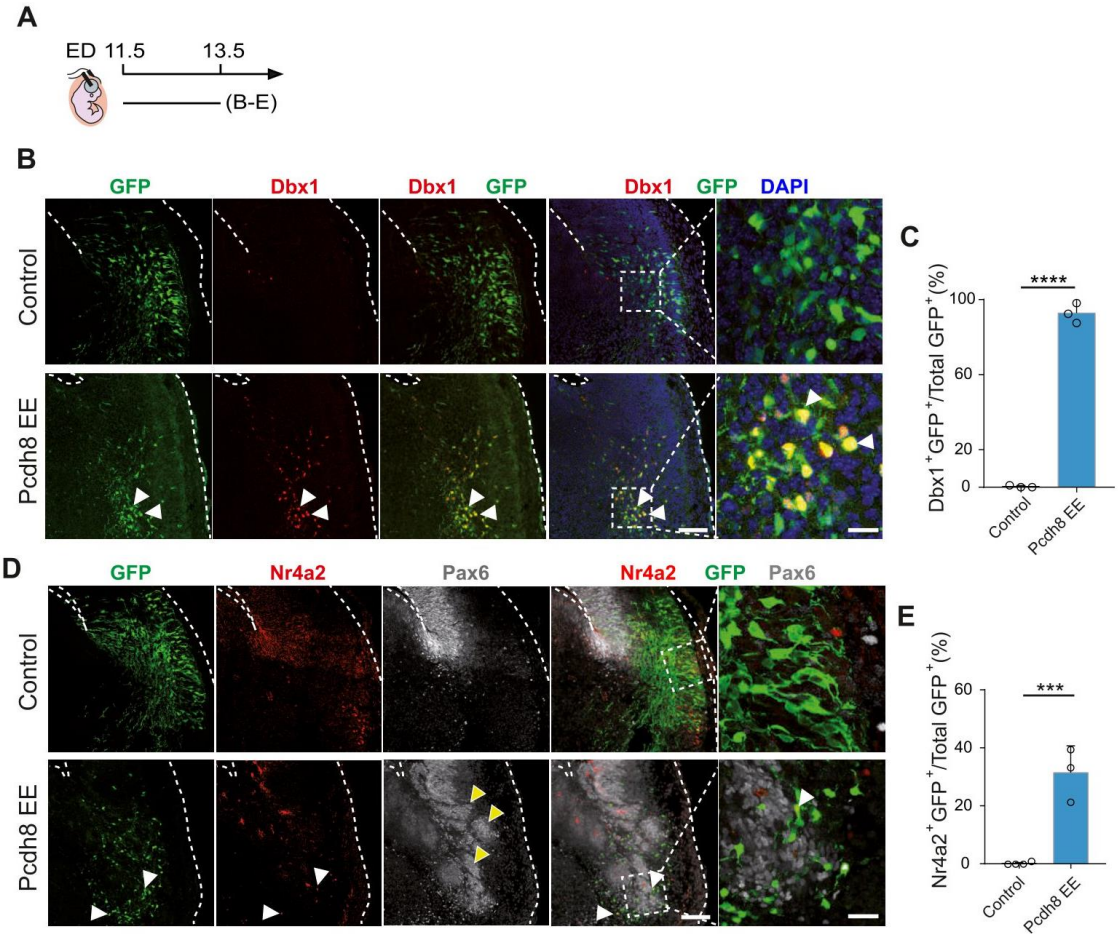

Figure 6. Pcdh8 EE induces Dbx1 and postmitotic markers expression

(A) Schematic timeline of the IUE. **(B)** Confocal images of GFP$^+$ (green) fluorescence in coronal sections of E13.5 mouse brains after IUE at E11.5 with a control vector or Pcdh8 EE co-labeled with Dbx1 (red) and DAPI (blue) counterstaining. White arrowheads indicate Dbx1$^+$GFP$^+$ cells. Scale bar: 200 µm. Dashed squares are shown at a higher magnification on the right. Scale bar: 50 µm. **(C)** Percentage of Dbx1$^+$GFP$^+$ cells over the total of GFP$^+$ cells. Data are mean ± SEM; circles indicate values from single animals (n=3 controls, n=3 Pcdh8 EE). Student's t-test: ****p< 0.0001. **(D)** Confocal images of GFP$^+$ (green) fluorescence in coronal sections of E13.5 mouse brains after IUE at E11.5 with a control vector or Pcdh8 EE co-labeled with Nr4a2 (red) and Pax6 (gray). Yellow and white arrowheads indicate disorganization of Pax6$^+$ and Nr4a2$^+$GFP$^+$, respectively. Scale bar: 200 µm. Higher magnification of the dashed squares is shown on the right. Scale bar: 50 µm. **(E)** Percentages of Nr4a2$^+$GFP$^+$ cells over the total of GFP$^+$ cells. Data are mean ± SEM; circles indicate values from single animals (n=3-4 controls, n=3-6 Pcdh8 EE). Student's t-test: ***p=0.0009 (E), ns, not significant (F).

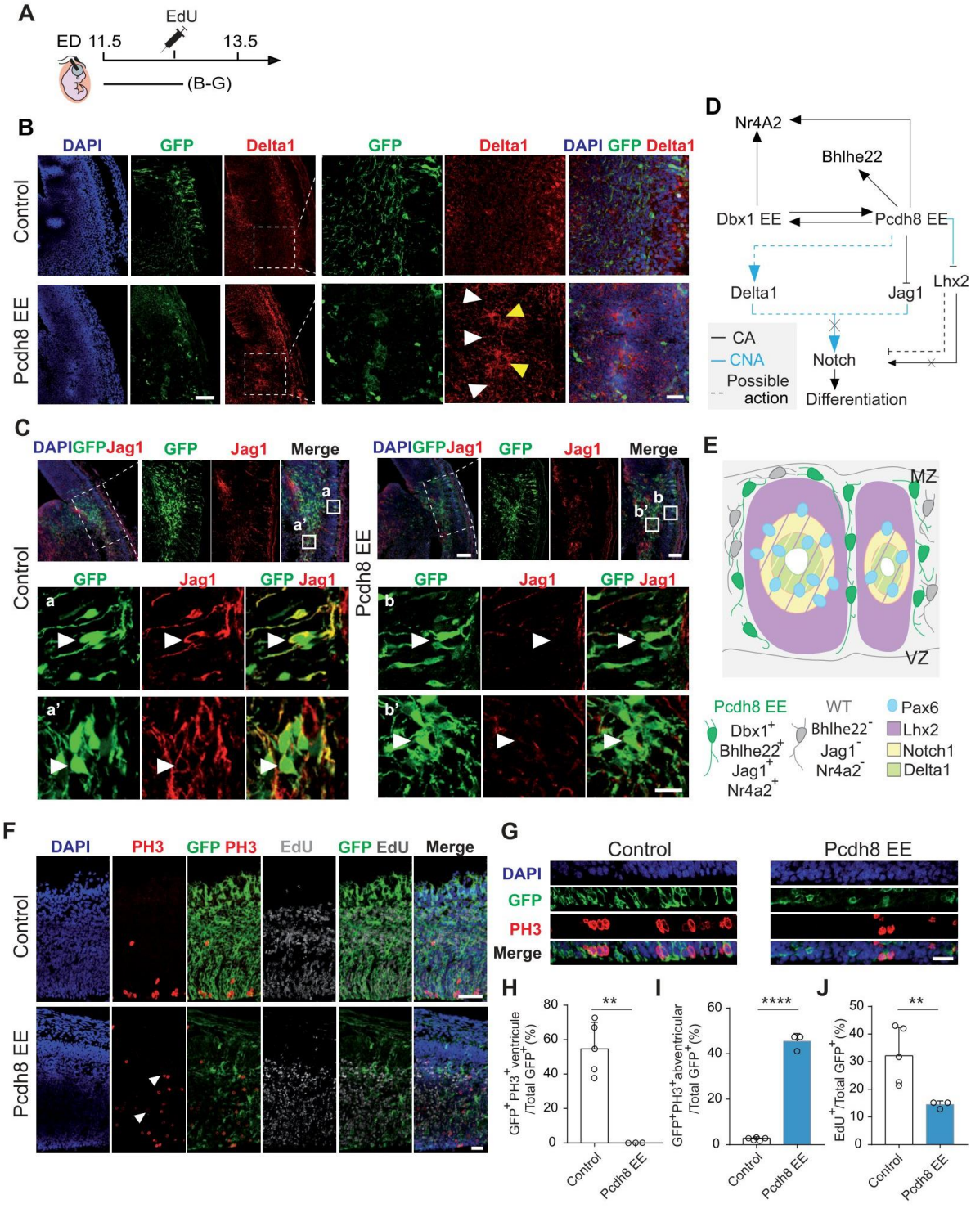

Figure 7. Pcdh8 EE alters the Notch1 pathway and cell cycle

(A) Schematic timeline of the IUE and EdU pulse. **(B)** Confocal images of GFP$^+$ (green) fluorescence in coronal sections of E13.5 mouse brains after IUE at E11.5 with a control vector or Pcdh8 EE co-labeled with Delta1 (red) and DAPI (blue) counterstaining. Scale bar: 200 µm. Higher magnification of the dashed squares is shown on the right. Yellow and white arrowheads indicate Delta1 accumulation signal or surrounding GFP$^+$ cells with low Delta 1 signal, respectively. Scale bar: 50 µm. **(C)** Confocal images of GFP$^+$ (green) fluorescence in coronal sections of E13.5 mouse brains after IUE at E11.5 with a control vector or Pcdh8 EE co-labeled with Jag1 (red) and DAPI (blue) counterstaining. Scale bars: 200 µm (top panels) and 100 µm (bottom panels). Higher magnification of the

dashed squares, control (a, a') and Pcdh8 EE (b, b'), is shown in the bottom panel. White arrowheads indicate representative cells of each condition. Scale bar: 25 µm. **(D)** Schema of the possible interactions between Dbx1, Pcdh8, Notch signaling and cell fate markers. CA, cell-autonomous; CNA, cell non-autonomous. **(E)** Cartoon showing composition of the rosette-like structures formed upon Pcdh8 EE. **(F)** Confocal images of GFP^+ (green) fluorescence in coronal sections of E13.5 mouse brains after IUE at E11.5 with a control vector or Pcdh8 EE followed by EdU administration 24h post IUE, co-labeled with PH3 (red), EdU (gray) and DAPI (blue) counterstaining. White arrowheads indicate $PH3^+$ cells outside the ventricular zone (VZ). Scale bar: 100 µm. **(G)** High magnification of the electroporated VZ in (F) with GFP (green), PH3 (red) and DAPI (blue) labeling. Scale bar: 50 µm. **(H-I)** Percentages of GFP^+PH3^+ cells over the total GFP^+ cells, either aligned at the VZ (H) or outside the VZ (I). Data are mean ± SEM; circles indicate values from single animals (n=3-5 mice/condition, 2 sections/mouse). Student's t-test: $^{**}p$=0.01 (H), $^{***}p$<0.001 (I). **(J)** Percentage of GFP^+EdU^+ cells over the total GFP^+ cells. Data are mean ± SEM; circles indicate values from single animals (n=3-5 mice/condition, 2 sections/mouse). Student's t-test: $^{**}p$=0.0087.

DISCUSSION

Pcdhs regulate cortical development from cell to tissue organization levels

TFs accomplish a key role in the formation and maintenance of different cell types during development. Indeed, changes in their levels (e.g. due to ectopic expression of Pax6, Lhx2 or Dbx1) alter initial programs of progenitor cells (Subramanian *et al.*, 2011; Pataskar *et al.*, 2016; Arai *et al.*, 2019). Our data demonstrates that changes in Dbx1 expression have an impact on adhesive properties of cells *via* Pcdh8, making it an essential element of cell identity sensitive to Pcdh levels. Interestingly, an emerging role of clustered Pcdhs (cPcdhs) in spatial and functional organization of neurons has recently been shown in the neocortex (Lv *et al.*, 2022). Indeed, it has been demonstrated that cPcdhs are expressed in patterned combinations by excitatory neurons that arise from the same progenitor cell. Furthermore, a specific surface pattern of cPCDHs is important for neuron positioning and its connections with other neurons (Lv *et al.*, 2022). Nevertheless, the regulatory mechanism regulating the expression of different patterns of cPcdhs genes has not been described. Here, we describe changes in spatiotemporal competence of the cortical neuroepithelium upon EE of the Dbx1 TF. These observations are consistent with the previously described role of endogenous Dbx1 expression working as a strong cell-fate determinant in different regions of the CNS (Pierani *et al.*, 2001; Bouvier *et al.*, 2010; Sokolowski *et al.*, 2016; Arai *et al.*, 2019). We found, that Dbx1 EE imparts different cell identities between E11.5 and E12.5 characterized by $Nr4a2^+$ expression at E11.5 and $Ctip2^+$ at E12.5. This correlates with induction of distinct set of Pcdhs, namely Pcdh8 at E11.5 and Pcdh9/Pcdh19 at E12.5. This suggests that progenitor cells competence differ and can give rise to daughter cells characterized by different sets of Pcdhs expressed on the surface. This can play a key role in segregating and organising cell types into the properly functioning brain areas. It has been shown that at early stages of spinal cord development specific cell adhesion molecules follow TFs expression in selected progenitor domains (Tsai *et al.*, 2020), determining patterning robustness of the tissue. In particular, we showed that Dbx1 EE within the LP led to the organization of transfected cells into Pcdh8-expressing aggregates with SP-like neuron characteristics ($Nr4a2^+/Reln^-/Calb2^-$). Moreover, Pcdh8 EE resulted in reorganization of multiple TFs expression crucial for correct dorso-ventral patterning (e.g. *Shh, Dbx1, Lhx2*). These results suggest that Pcdhs expression is time-restricted and that Pcdh8 can alter the spatial organisation of TFs and, consequently, proper cortical development.

Adhesion is an important component of the cell identity

Dbx1 was previously shown to function as a potent determinant of cell identity in the mouse spinal cord (Pierani *et*

al., 2001). During early development, Dbx1-expressing domains are present at the borders of the pallium and subpallium, notably the VP/PSB and septum (Bielle *et al.*, 2005; Griveau *et al.*, 2010). Interestingly, we detected Pcdh8 transcripts in VP and septum Dbx1-expressing, and Dbx1-derived cells in the postmitotic compartment. Thus, suggesting of possible synergic role of Dbx1 and Pcdh8 in cell identity determination. Indeed, Pcdh8 KD in Dbx1 EE cells reversed induction of Nr4a2 expression supporting that Pcdh8 is in part responsible for Nr4a2 expression and SP-like phenotype of Dbx1-derived lineages (Arai *et al.*, 2019; Moreau *et al.*, 2021). Moreover, further analysis showed the action of Pcdh8 KD on downregulation (Dbx1 EE + Pcdh8 KD) and upregulation (Pcdh8 EE) of Dbx1, thus pointing to Pcdh8 as a post-transcripitional modulator of Dbx1 expression. Finally, Pcdh8 EE cells were characterised by coexpression of Dbx1 and postmitotic markers such as Nr4a2 or Bhlhe22, showing novel and important regulatory function of adhesion molecule on TF expression and cell fate.

Crosstalk between Pcdh8 and TFs influence tissue morphogenesis

Multiple studies showed that disturbance of TF expression, i.e. Lhx2 or/and Pax6, results in re-patterning of TFs expression domains (Mangale et al., 2008; Roy et al., 2013; Godbole et al., 2017) and tissue overgrowth (Mangale et al., 2008). Similarly, we observed that shift of the septum-restricted or/and ventro-lateral expression of Pcdh8 into more dorsal pallium resulted in disturbance of *Lhx2* and Pax6 TFs expression in progenitor cells. This was followed by formation of rosette-like structures with new proliferative centres rich in Ncad. Moreover, we observed a shift of the subpallial progenitor TF marker *Gsx2* into the DP and postmitotic Bhlhe22 one being expressed on the outside of the rosettes, both in a CA or CNA manner. These observations are consistent with studies on disturbance of the Gsx2-Pax6-Dbx1 border at the PSB (Cocas et al., 2011) or hem-antihem balance due to Lhx2 dysregulation which led to dramatic impairment in DV organization and in consequence deformation of the developing pallium (Godbole et al., 2017). Thus, our work adds Pcdh8 as a new organizer of the DV axis. This can be explained by an action of Pcdh8 on TF expression by activation of intracellular signalling cascades *via* its intracellular domain (ICD). Notably, *cis*-binding of Pcdh8 to Ncad, whereby Pcdh8 ICD activates the MAP kinase (MAPK) TAO2β has been previously described (Yasuda et al., 2007). Interestingly, MAPK are key mediators of eukaryotic transcriptional responses to extracellular stimuli (Zarubin and Han, 2005; Whitmarsh, 2007). Notably, we found that Dbx1 EE is shut down *via* a Pcdh8 mediated mechanisms at post transcriptional levels. Thus, it would be interesting to further investigate the action of Pcdh8 on transcriptional and posttranscriptional mechanisms. Overall, these results show that Pcdh8, normally strongly expressed ventrally to the PSB, when ectopically expressed at or dorsal to the PSB can significantly influence DV organisation and activity of several TFs in CA and CNA manners.

Notch signalling as a downstream partner of Pcdhs

Tight control of both temporal and spatial patterning of neuronal populations is regulated by the Notch signalling pathway (Wang *et al.*, 2015; Ware *et al.*, 2016). Notch1 inactivation has been associated with acceleration of neuronal differentiation both in the mouse spinal cord and developing brain (Tokunaga *et al.*, 2004; Yang *et al.*, 2006; Kong *et al.*, 2015). Furthermore, it controls the number of neural progenitor cells that can exit the cell cycle and undergo differentiation (Moore and Alexandre, 2020). We showed that Pcdh8 influences cell cycle exit and postmitotic fate acquisition. Moreover, we found that Pcdh8 represses Notch1 signalling ligands (Jag1 and Dll1) in

CA and CNA manner respectively, thus suggesting this might influence differentiation. Interestingly, Dbx1 was also shown to influence Jag1 expression in the spinal cord (Skaggs *et al.*, 2011) and cell cycle exit (García-Moreno *et al.*, 2018). These findings indicate that the Notch pathway is a relevant candidate for Pcdh8 and Dbx1 cooperative function, which pushes progenitors out of the cell cycle to premature differentiation.

In summary, our study proposes adhesion molecules, in particular Pcdh8, as novel players in the processes of pallium formation and cell fate determination. Most of all, we show that Pcdh8 through a bidirectional regulatory mechanism with the Dbx1 TF can modulate cell cycle dynamics, cell fate and, in consequence, organization of the developing brain. Moreover, we identified Notch signaling as a potential downstream partner of Pcdh8, shedding light on a possible regulatory mechanism behind this process.

SUPPLEMENTAL INFORMATION

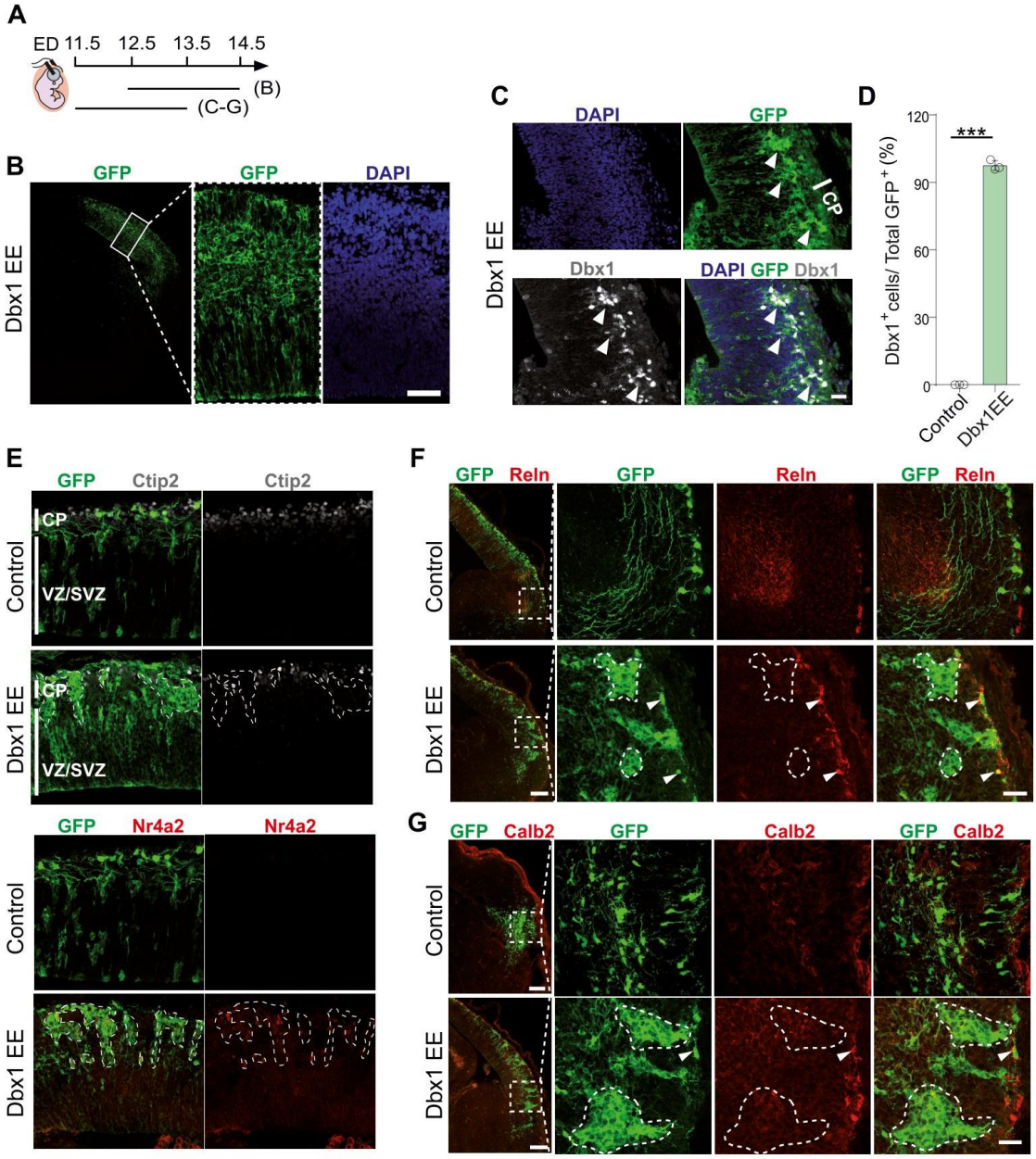

Supplementary Figure 1. *Dbx1 EE at E11.5 induces the formation of cell aggregates composed of SP-like neurons.*

(A) Schematic timeline of the IUE. **(B)** Confocal images of GFP$^+$ (green) fluorescence in coronal sections of E14.5 mouse brains upon IUE at E12.5 with Dbx1 EE and DAPI (blue) counterstaining. Scale bar: 100 µm. **(C)** Confocal images of GFP$^+$ (green) fluorescence in coronal sections of E13.5 mouse brains after IUE at E11.5 with Dbx1 EE, co-labeled with Dbx1 (gray) and DAPI (blue) counterstaining. White bar shows the cortical plate (CP). White arrowheads indicate Dbx1$^+$GFP$^+$ cells. Scale bar: 50 µm. **(D)** Percentage of Dbx1$^+$GFP$^+$ cells over the total of GFP$^+$ cells. Data are mean ± SEM; circles indicate values from single animals (n=3 mice/condition). Student's t-test: ***p<0.001. **(E)** Confocal images of GFP$^+$ (green) fluorescence in coronal sections of E13.5 mouse brains upon IUE at E11.5 with a control vector or Dbx1 EE, co-labeled with Ctip2 (gray) and Nr4a2 (red). White bars show the CP and the ventricular/subventricular zones (VZ/SVZ). Dashed areas mark Dbx1$^+$ aggregates. Scale bar:

50 µm. **(F)** Confocal images of GFP$^+$ (green) fluorescence in coronal sections of E13.5 mouse brains upon IUE at E11.5 with a control vector or Dbx1 EE, co-labeled for Reln (red). Scale bar: 200 µm. Right panel: Higher magnification of the dashed squares. Scale bar: 50 µm. Dashed area show examples of Dbx1-EE aggregates. White arrowheads indicate GFP$^+$Reln$^+$ cells localized outside of the aggregates. **(G)** Confocal images of GFP$^+$ (green) fluorescence in coronal sections of E13.5 mouse brains upon IUE at E11.5 with a control vector or Dbx1 EE, co-labeled for Calb2 (Calr) (red). Scale bar: 200 µm. Right panel: Higher magnification of the dashed squares. Scale bar: 50 µm. Dashed area show examples of Dbx1-EE aggregates. White arrowheads indicate GFP$^+$Calb2$^+$ cells localized outside of the aggregate.

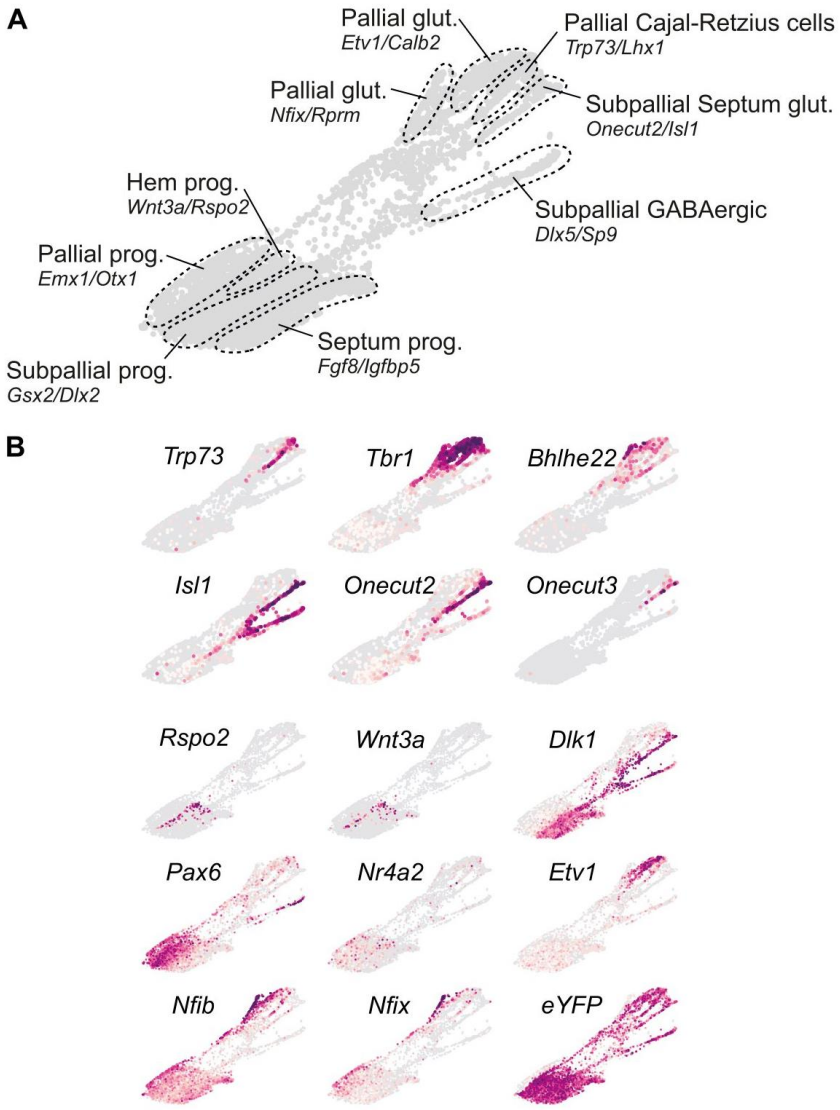

Supplementary Figure 2. *Distinct lineages and differentiation trajectories are characterized around the septum.*

(A) SPRING dimensionality reduction of the septum dataset showing the distinct types of progenitors and neurons that were identified. Selected marker genes are indicated for each population. **(B)** SPRING dimensionality reduction plots indicating the expression levels of some of the genes that were used for annotating the dataset.

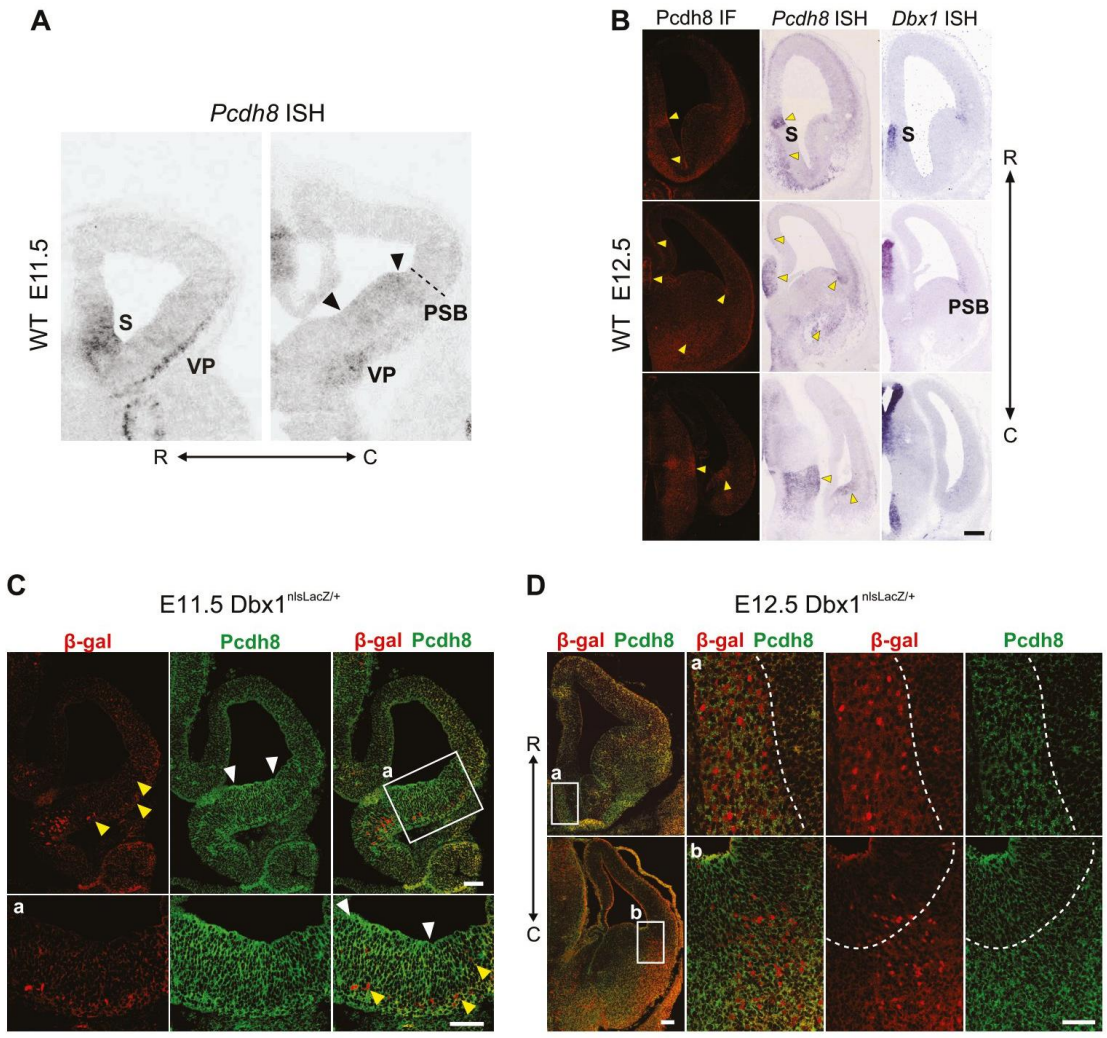

Supplementary Figure 3. *Pcdh8 and Dbx1 display interrelated expression patterns in the developing telencephalon.*

(A) Bright-field images of *in situ* hybridization (ISH) for *Pcdh8* performed on rostral (R) and caudal (C) brain sections of E11.5 *wild-type* (WT) mice. Double arrow line indicates the R-C axis. Black arrowheads indicate high levels of *Pcdh8* expression. S, septum; PSB, pallial-subpallial boundary; VP, ventral pallium. **(B)** Left: Confocal images of Pcdh8^{+} (red) immunofluorescence (IF) in coronal sections of E12.5 WT mouse brains. Right: Bright-field images of ISH for *Pcdh8* and *Dbx1* performed on E12.5 WT mouse brain sections. Double arrow line indicates the R-C axis. Yellow arrowheads indicate strong matching of Pcdh8 signal between IF and ISH validating the anti-Pcdh8 serum. Scale bar: 100 µm. **(C-D)** Confocal images of β-gal (red) and Pcdh8 (green) co-labeled on coronal brain sections of E11.5 (C) and E12.5 (D) *Dbx1$^{nlsLacZ/+}$* mice. Yellow arrowheads show β-gal^{+}Pcdh8^{+} cells, white arrowheads indicate Pcdh8^{+} area. Higher magnification of squares (a) and (b) is shown in the bottom of the low magnification images. Dashed lines show the borders of stronger Pcdh8 staining. Scale bars: 200 µm (low magnification C and D), 100 µm (high magnification C and D).

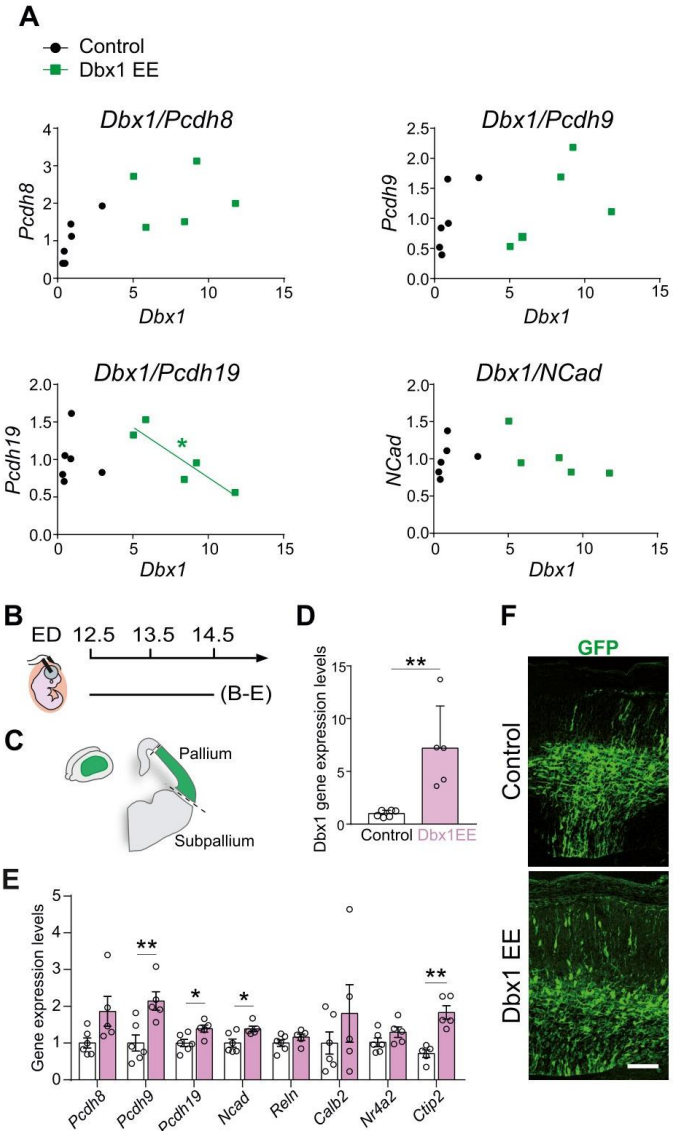

Supplementary Figure 4. *Dbx1 EE at E12.5 induces expression of different sets of genes in comparison to IUE at E11.5.*

(A) Graphs of qPCR results upon IUE (E11.5-E13.5) with a control vector or Dbx1 EE showing no (*Dbx1/Pcdh8*; *Dbx1/Pcdh9*; *Dbx1/Ncad*) or negative (*Dbx1/Pcdh19*) gene expression correlation. **(B)** Schematic timeline of the IUE. **(C)** Electroporated region dissection scheme. **(D, E)** qPCR quantification of the average *Dbx1* (D) or *Pcdh8, Pcdh9, Pcdh19, Ncad, Reln, Calb2, Nr4a2* and *Ctip2* (E) gene expression upon IUE (E12.5-E14.5) with control vector or Dbx1 EE normalized to the control. Data are mean ± SEM; circles indicate values from single sample (n=6 controls, n=5 Dbx1 EE). Student's t-test: $^{**}p$=0.0014 (D), $^{*}p \leq 0.05$; $^{**}p \leq 0.01$ (E). **(F)** Confocal images of GFP^{+} (green) fluorescence in coronal sections of E14.5 mouse brains upon IUE at E12.5 with a control vector or Dbx1 EE. Scale bar: 100 µm.

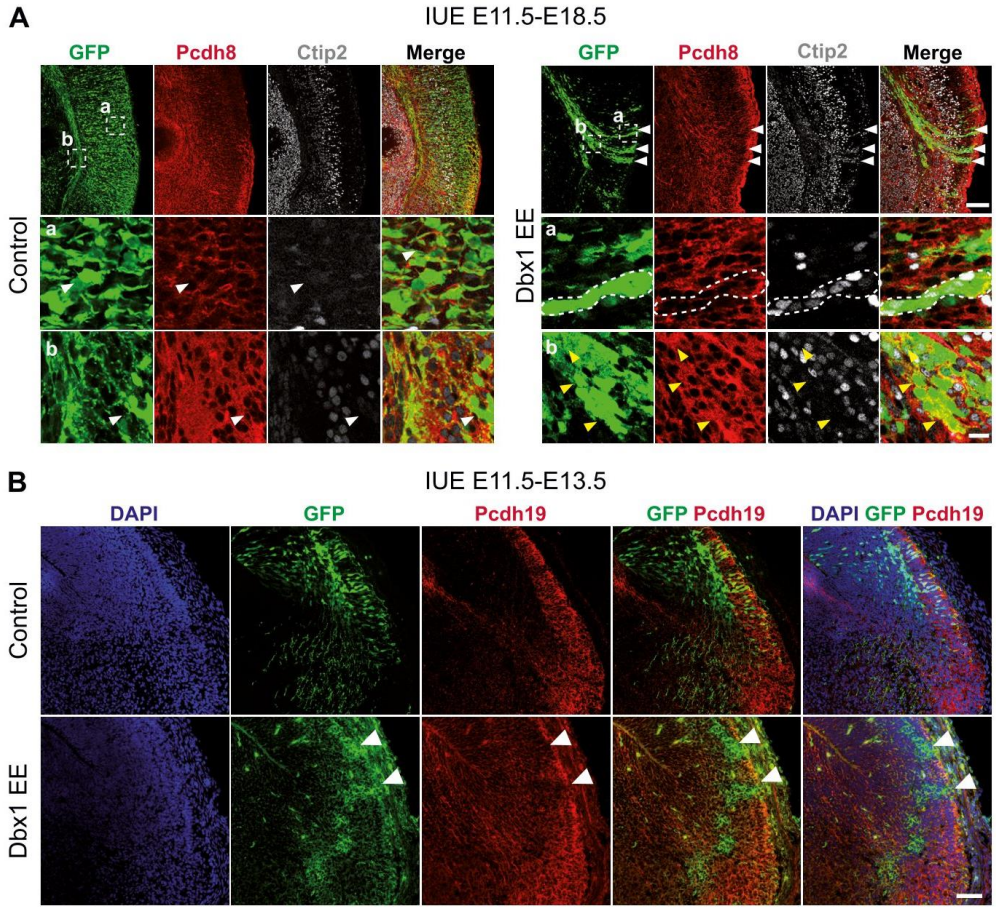

Supplementary Figure 5. *Dbx1 EE at E11.5 affects cell identity and adhesion.*

(A) Confocal images of GFP$^+$ (green) fluorescence in coronal sections of E18.5 mouse brain cortices upon IUE at E11.5 with a control vector or Dbx1 EE, co-labeled for Ctip2 (gray) and Pcdh8 (red). Higher magnification of the dashed squares (a and b) is shown in the bottom. White arrowheads in control indicate GFP$^+$Ctip2$^-$Pcdh8$^-$ cells and in Dbx1 EE indicate strongly adherent 'streams' of GFP$^+$ cells. Dashed area in (a) shows a group of Dbx1 EE Ctip2$^+$Pcdh8^{low} cells in the cortical plate (CP). Yellow arrowheads indicate Dbx1 EE Ctip2$^-$Pcdh8^{high} cells below the CP. Scale bars: 200 μm (top), 25 μm (bottom). **(B)** Confocal images of GFP$^+$ (green) fluorescence in coronal sections of E13.5 mouse brain cortices upon IUE at E11.5 with control vector or Dbx1 EE, labeled for Pcdh19 (red) with DAPI (blue) counterstaining. White arrowheads show Pcdh19$^-$ aggregates induced by Dbx1 EE. Scale bar: 100 μm.

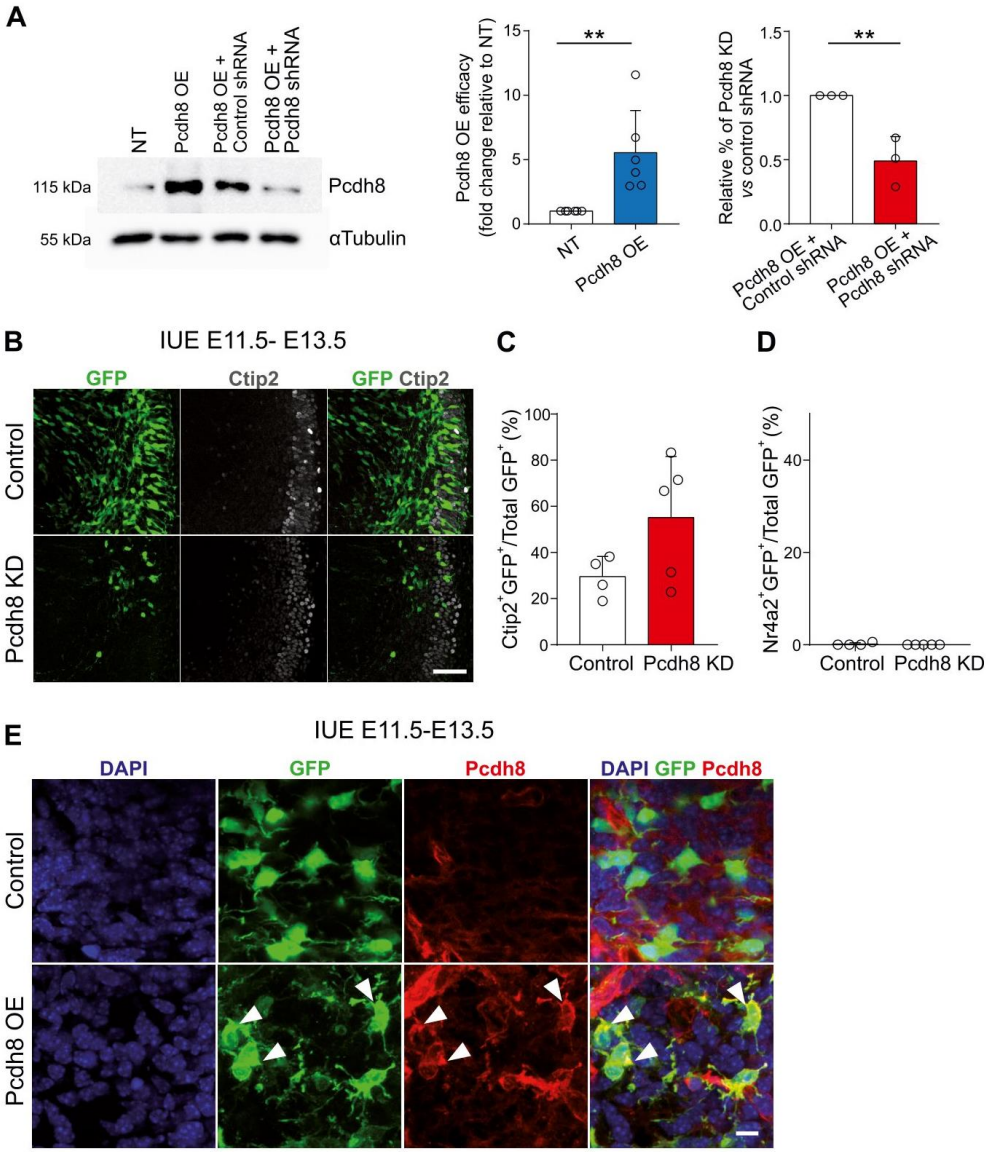

Supplementary Figure 6. *Pcdh8 KD does not affect cell identity.*

(A) Representative immunoblotting (left) and densitometric analysis (right) of Pcdh8 signal from cell lysates of 48h post-transfected HEK293T cells with the following conditions: NT – not transfected; Pcdh8 OE (overexpression) vector; Pcdh8 OE + control shRNA; Pcdh8 OE + Pcdh8 shRNA. Pcdh8 signal was normalized to αTubulin (n=3-6 independent transfections). Data are mean ± SEM; each circle represents one transfection. Student's t-test: **$p \leq 0.01$. **(B)** Confocal images of GFP$^+$ (green) fluorescence in coronal sections of E13.5 mouse brains after IUE at E11.5 with a control shRNA or Pcdh8-targeted shRNA (Pcdh8 KD), co-labeled with Ctip2 (gray). Scale bar: 100 µm. **(C, D)** Percentage of Ctip2$^+$GFP$^+$, Nr4a2$^+$GFP$^+$ cells over the total of GFP$^+$ cells, respectively. Data are mean ± SEM; circles indicate values from single animals (n=3-6 controls, n=4-5 Pcdh8 KD). Student's t-test: $p>0.05$ –not significant **(E)** Confocal images of GFP$^+$ (green) fluorescence in coronal sections of E13.5 mouse brains upon IUE at E11.5 with control vector or Pcdh8 EE, co-labeled with Pcdh8 (red) and DAPI (blue) counterstaining. White arrowheads indicate cells with overexpression of Pcdh8. Scale bar: 50 µm.

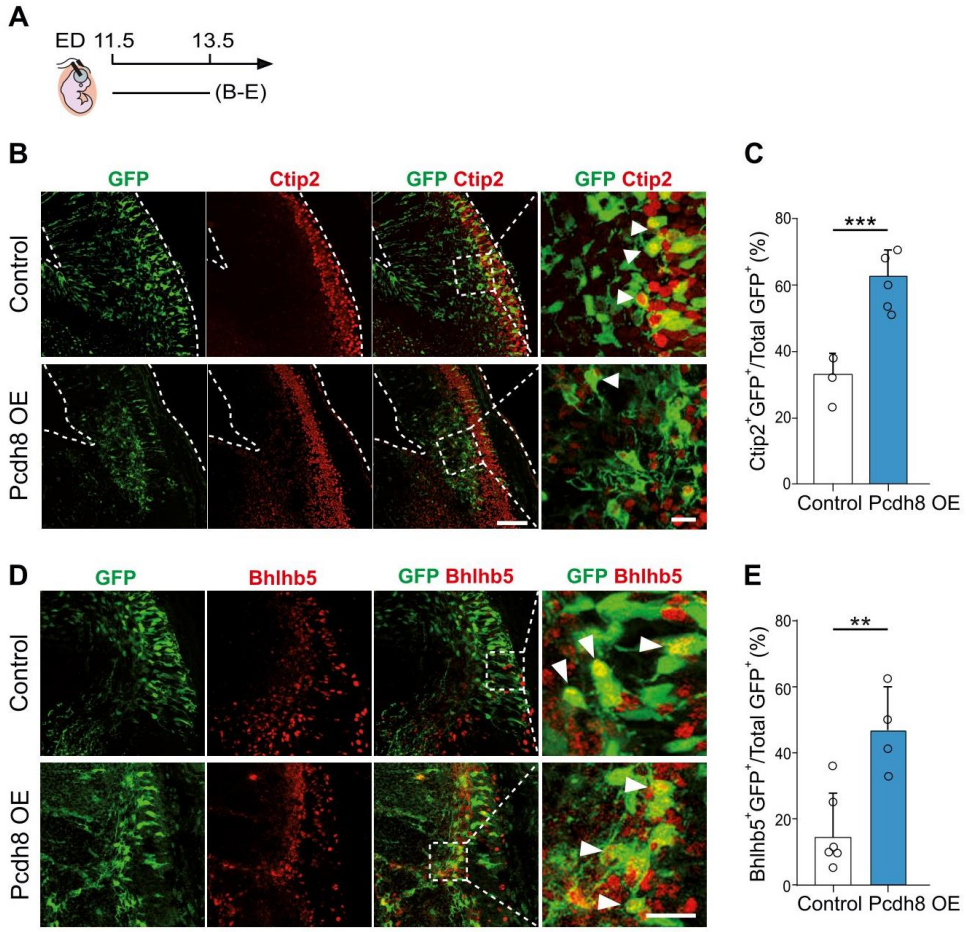

Supplementary Figure 7. *Pcdh8 EE induce Ctip2- and Bhlhe22-expressing cells.*

(A) Schematic timeline of the IUE. **(B)** Confocal images of GFP$^+$ (green) fluorescence in coronal sections of E13.5 mouse brains after IUE at E11.5 with control vector or Pcdh8 EE co-labeled with Ctip2 (red). Scale bar: 150 µm. Higher magnification of the dashed squares is shown on the right. Scale bar: 50 µm. **(C)** Percentage of Ctip2$^+$GFP$^+$ cells over the total of GFP$^+$ cells. Data are mean ± SEM; circles indicate values from single animals (n=3 controls, n=5 Pcdh8 EE). Student's t-test: ***p=0.0018. **(D)** Confocal images of GFP$^+$ (green) fluorescence in coronal sections of E13.5 mouse brains upon IUE at E11.5 with a control vector or Pcdh8 EE co-labeled with Bhlhe22 (red). Scale bar: 150 µm. Higher magnification of the dashed squares is shown on the right. Scale bar: 50 µm. **(E)** Percentage of Bhlhe22$^+$GFP$^+$ cells over the total of GFP$^+$ cells. Data are mean ± SEM; circles indicate values from single animals (n=6 controls, n=4 Pcdh8 EE). Student's t-test: **p=0.0054.

ACKNOWLEDGMENTS;

We thank E. Panafieu, Animalliance and the Imagine Institute animal house staff for mouse care and technical help. We also appreciate advice in cloning process and donation of pStrike plasmid by P. Billuart. Furthermore, we thank Stéphane Nedelec and Sophie Thomas for their help in the experiments not included in this manuscript. This work was supported by Fondation pour la Recherche Médicale; Number of the project: SPF20170938863, Fundation Fyssen; Number of the project: CH9147, CDEIGENT/2021/005 to A.W.C., by grants from the Agence Nationale de la Recherche (ANR-2011-BSV4-023-01, ANR-15-CE16-0003-01 and ANR-20-CE16-0001-01), FRM (Equipe FRM DEQ20130326521 and EQU201903007836) to A.P; and state funding from the Agence Nationale de la Recherche under ‘‘Investissements d’avenir’’ program (ANR-10-IAHU-01) to the Imagine Institute A.P. is a CNRS (Centre National de la Recherche Scientifique) Investigator.

CO-AUTHORS CONTRIBUTION

Conceptualization, A.W.C, F.C., A.P.; Methodology A.W.C., F.C and A.P.; Investigation, A.W.C, J.G.J., S.F, M.X.M, Y.S., E.D., J.G.M., U.B.; Data Curation, A.W.C.; Writing – Original Draft, A.W.C. and A.P.; Writing – Review & Editing, A.W.C., S.F., F.C. and A.P.; Visualization, A.W.C., M.X.M. and F.C.; Supervision, A.P.; Project Administration, A.W.C. and A.P.; Funding Acquisition, A.W.C and A.P.

DECLARATION OF INTEREST

We wish to confirm that there are no known conflicts of interest associated with this publication and there has been no significant financial support for this work that could have influenced its outcome.

STAR METHODS

REAGENT or RESOURCE	SOURCE	IDENTIFIER
Antibodies		
αTubulin (Polyclonal Rabbit)	Invitrogen	PA529444
Bhlhe22 (Monoclonal Guinea Pig)	Pierani et al., 2001	N/A
β-Gal (Polyclonal Chicken)	Abcam	ab9361
Ctip2 (Monoclonal Rat)	Abcam	ab18465
DAPI (4', 6-diamidino-2-phenylindole)	Sigma	D9542
Dbx1 (Polyclonal Rabbit)	Pierani et al., 2001	N/A
Delta 1(Polyclonal Rabbit)	Santa Cruz	SC-9102
Gfp (Polyclonal Chicken)	Aves labs	GFP-1020
Jag1 (Polyclonal Goat)	Santa Cruz	SC-6011
Ncad (Monoclonal Mouse)	BD Bioscience	610921
Nr4a2 (Nurr1) (Polyclonal Goat)	R&D systems	AF2156
Pax 6 (Polyclonal Mouse)	Biotech	12323-1-AP
Pcdh8 (Monoclonal Mouse)	Novus Bio	H000051100-M01
Pcdh19 (Polyclonal Rabbit)	Abcam	Ab191198
pH3 (Polyclonal Rabbit)	Millipore	06-570
Tbr2 (Polyclonal Chicken)	Millipore	AB15894

Alexa-488 Donkey Anti-Mouse	Molecular Probes	A-21202
Alexa-488 Donkey Anti-Chicken	Jackson Laboratories	703-545-155
Alexa-555 Goat Anti-Guinea Pig	Molecular Probes	A-21435
Cy3 Donkey Anti-Mouse	Jackson Laboratories	715-165-151
Cy3 Donkey Anti-Rabbit	Jackson Laboratories	711-165-152
Cy3 Donkey Anti-Goat	Jackson Laboratories	705-165-003
Cy5 Donkey Anti-Rat	Jackson Laboratories	712-175-153
Cy5 Donkey Anti-Rabbit	Jackson Laboratories	711-175-152
Cy5 Donkey Anti-Guinea Pig	Jackson Laboratories	706-175-148
Biotin-SP-Conjugated AffiniPure Goat Anti-Mouse	Jackson Laboratories	115-065-146
HRP-conjugated secondary anti-mouse	Jackson Laboratories	115-035-008
HRP-conjugated secondary anti-rabbit	Jackson Laboratories	111-035-008
Bacterial and Virus Strains		
One Shot™ TOP10 competent E. coli	Invitrogen	C404010
Biological Samples		
CHEMICALS, PEPTIDES, AND RECOMBINANT PROTEINS		
Critical Commercial Assays		
Click iT EdU Alexa Fluor 647 Imaging Kit	Invitrogen	C10340
DIG-RNA labeling kit	Roche	11277073910
GoTag qPCR Master Mix	Promega	A6001
RevertAid First Strand cDNA Synthesis Kit	Thermo Scientific	K1622
Chromium Single Cell 3' Library & Gel Bead Kit	10x Genomics	PN-120267
Neural Tissue Dissociation Kit (P)	Miltenyi Biotec	130-092-628
DNase I, RNase-free	Thermo Scientific	EN0521
Deposited Data		
Raw and analyzed single-cell sequencing data	This paper	GEO: GSE229603
R codes for analysis	This paper	https://fcauseret.github.io/septum/
Experimental Models: Cell Lines		
HEK293T	ATCC	CRL-3216
Experimental Models: Organisms/Strains		
C57BL/6RJ	Janvier Labs France	SC-C57J-F
Dbx1^{LacZ}	(Pierani et al., 2001)	N/A
Rosa^{26YFP}	(Srinivas et al., 2001)	N/A
Rosa^{26tdTomato}	(Madisen et al., 2010)	N/A
Oligonucleotides		
ISH: Dbx1	Pierani et al., 2001	N/A
ISH: Pcdh8-forward AAGAAGGAGCCTTACGGTGC	This paper	N/A
ISH: Pcdh8-reverse TGCTACCAGGAGGGGATTCA	This paper	N/A
ISH: Bhlhe22-forward TTAGTCGCCTACCTCAACCAA	This paper	N/A
ISH: Bhlhe22-reverse TTTCTCCTGGCTCAGAATCAAG	This paper	N/A

qPCR:Dbx1-forward CTTGAAGGACTCGCAGGTGA	This paper	N/A
qPCR: Dbx1-reverse TTTGTGGGAAGGGTCTGCTC	This paper	N/A
qPCR: Pcdh8-forward ATGTTCGACGTGCTCACCTT	This paper	N/A
qPCR: Pcdh8–reverse CTCGAAGTGACAGGCGCTTT	This paper	N/A
qPCR: Pcdh9-forward ACCCTTTCCAAACGCTCCTC	This paper	N/A
qPCR: Pcdh9-reverse GAGGTCCATCTGTCTGGTGTG	This paper	N/A
qPCR: Pcdh19-forward CATCACTTGTCTCCTCGGCT	This paper	N/A
qPCR: Pcdh19-reverse TCAGCGATTCTCTTTCCCCTT	This paper	N/A
qPCR: Ncad-forward GGGTGTCCAAGGGTGACAAG	This paper	N/A
qPCR: Nacd-reverse TTGCTGAATTTCACTTGCAAAGC	This paper	N/A
qPCR: Nr4a2-forward GCTCAGCTCGGCGGTC	This paper	N/A
qPCR: Nr4a2-reverse CGTCAGATCTCCCTGCCCA	This paper	N/A
qPCR: Reln-forward TTACAACGTCCCCCTGGAAG	This paper	N/A
qPCR: Reln-reverse TAGGACGACCTCCACATGGT	This paper	N/A
qPCR: Calr-forward AGCACTTTGATGCTGACGGA	This paper	N/A
qPCR: Calr-reverse TGGACATCATGCCAGAACCC	This paper	N/A
qPCR: Ctip2-forward GGAGAACATTGCAGGGCCG	This paper	N/A
qPCR: Ctip2-reverse GGGAAACAGGGTGGGAGAAC	This paper	N/A
qPCR: GAPDH-forward: TGACGTGCCGCCTGGAGAAAC	This paper	N/A
qPCR: GAPDH-reverse: CCGGCATCGAAGGTGGAAGAG	This paper	N/A
Recombinant DNA		
pCAGGS-ires-EGFP	Addgene	#32482
psiSTRIKE-CAG-ires-GFP	Gift from Pierre Billuart	Hu et al., 2016
Pcdh8 shRNA Top Strand: ACCGGCGTGTGCTAGATGCCAATGACGAAT CATTGGCATCTAGCACACGCCTTTT	This paper	N/A

Pcdh8 Scrambled shRNA Top Strand: ACCGGTGGGAATCGCGCTTACAGTACGAAT ACTGTAAGCGCGATTCCCACCTTT	This paper	N/A
Software and Algorithms		
Adobe Photoshop	Adobe Systems Incorporated	https://www.adobe.com/products/photoshop.html
Excel	Microsoft	Microsoft
Graph Prism	GraphPad Software	https://www.graphpad.com/scientific-software/prism/
Adobe Illustrator	Adobe Systems Incorporated	https://www.adobe.com/products/illustrator.html
Image J	Schneider et al., 2012	https://imagej.nih.gov/ij/
NDP Viewer		U12388-01
Image Lab™ software	Biorad	https://www.bio-rad.com/
Other		
NEPA21 electroporator	Nepagene	NEPA21
In-Fusion® HD Cloning	Takara Bio	102518
RevertAid First Strand cDNA Synthesis Kit	Thermo Fisher	K1622
Go Tag qPCR Master Mix	Promega	A6001
DAPI (4', 6-diamidino-2-phenylindole)	Invitrogen	# D1306
EdU (5-ethynyl-2'-deoxyuridine)	Invitrogen	#E10187
DMEM	Gibco	31966021
Opti-MEM Reduced Serum Medium	Gibco	11058021
Opti-MEM Reduced Serum Medium, Glutamax Supplement	Gibco	51985026
Fetal Bovine Serum (FBS)	Gibco	10270106
Penicillin-Streptomycin (P/S)	Gibco	15140122
Lipofectamine 2000	Invitrogen	11668019
PI cocktail (cOmplete™ tablets)	Roche	4693159001
BCA protein assay reagent kit	Thermo Fisher	23227
TRIzol Reagent	Invitrogen	15596-026
Vilo Kit cDNA synthesis	Invitrogen	11754050
SDS-PAGE on 3-8% tris-acetate gels (NuPAGE, Invitrogen)	Thermo Fisher	EA03785BOX
NuPAGE™ Antioxidant	Invitrogen	NP0005
NuPAGE™ LDS Sample Buffer (4X)	Invitrogen	NP0007
NuPAGE™ Sample Reducing Agent (10X)	Invitrogen	NP0004
NuPAGE™ Tris-Acetate SDS Running Buffer (20X)	Invitrogen	LA0041
NuPAGE™ Transfer Buffer (20X)	Invitrogen	NP00061
Skimmed milk	Régilait	NA
Nitrocellulose membranes 0.45 (Amersham)	GE Healthcare	GE10600002
Protein standard (HiMark 31-460 kDa)	Invitrogen	LC5699
SuperSignal West Pico Chemiluminescent	Thermo Fisher	34580

Chloroform	VWR	22711.290
Paraformaldehyde (PFA)	VWR	28794.295
Sodium Chloride (NaCl)	VWR	28244.295
NP-40	Sigma	18896
Sodium deoxycholate	Sigma	30970
SDS solution 20%	Sigma	05030-1L-F
Tris-HCl	Sigma	T3253
Tween-20	VWR	28829.296
Horse serum (HS)	Gibco	16050122
In-Fusion HD Cloning Kit	Takara Bio	639650
Tissue-Tek O.C.T compound	Sakura	4583
Vectashield Mounting medium	Vector Labs	H-1000

Table 1. List of reagents used in the study.

Animals

The following mouse lines were used and maintained on a *C57BL/6J* background: *Dbx1*^{LacZ} (Pierani et al., 2001), *Rosa26*^{YFP} (Srinivas et al., 2001) and *Rosa26*^{tdTomato} (Madisen et al., 2010). All animals were handled in strict accordance with good animal practice as defined by the national animal welfare bodies, and all mouse work was approved by the Veterinary Services of Paris (Authorization number: 75–1454) and by the Animal Experimentation Ethical Committee Paris-Descartes(CEEA-34) (Reference: 2018012612027541).

In utero electroporation

The procedure was carried out following previously published protocols (Szczurkowska *et al.*, 2016; Arai *et al.*, 2019). Briefly, to ensure the welfare of the used animals, 30 min before the surgery 50 µg/kg of Buprenorphine followed by 5 mg/kg Ketoprofen post-surgery subcutaneous administration were performed. *Wild-type C57BL/6J* pregnant mice at E11.5 or E12.5 were subjected to incision under anesthesia with Isoflurane (AXIENCE SAS), and the uterine horns were exposed onto 1X phosphate-buffered saline (PBS)-moistened cotton gauze. Embryos were visualized using appropriate flexible light sources through the uterus. Plasmid DNAs mixed with a filtered Fast Green dye were injected into the lateral ventricle through a glass capillary. A pair of 3 mm electrodes was applied to the embryos through the yolk sac, and a series of square-wave current pulses (25 V, 50 ms) was delivered for six times at 950 ms intervals using a pulse generator (NEPA21, NEPAGENE). Uterine horns were repositioned into the abdominal cavity, and the abdominal wall and skin were sutured. The concentration of plasmid DNAs used were between 1-3 mg/ml. The animals were checked in the post-surgery care room (heating pad, wet food and, if necessary, additional dose of painkiller was administrated).

Plasmid DNA Cloning

For the study we used a pCAGGS-HA-mouseDbx1-ires-NLS-EGFP vector previously published in Arai et al. (Arai *et al.*, 2019). The Pcdh8 overexpression sequence was subcloned into the pCAGGS vector backbone using In-Fusion® HD Cloning (Takara Bio) accordingly to the manufacturer's instructions.

Pcdh8 shRNA and scrambled shRNA sequences were subcloned into psiSTRIKECAG-ires-GFP vectors (a gift from Dr. Billuart) using In-Fusion® HD Cloning (Takara Bio) accordingly to the manufacturer's instructions.

Immunofluorescence

Mice were sacrificed by cervical dislocation and embryos were collected and fixed at 4ºC for 2h (E11.5-E12.5), 2.5h (E13.5), 3h (E14.5), 4h (E18.5) in 4% paraformaldehyde (PFA)/PBS, washed in PBS 3x1h at 4ºC, cryoprotected in 30% sucrose/PBS overnight at 4ºC, and embedded in Tissue-Tek O.C.T compound (Sakura Finetek, Europe). Coronal cryosections of mouse embryos (20 µm: E11.5-E14.5; 25 µm: E18.5) were blocked with 0.2% Triton X-100 in 10% horse serum/1X PBS for 30 min. For Pcdh8 immunostaining, before blocking, sections were incubated for 10 min at 95ºC in antigen retrieval solution (10mM sodium citrate, pH 6.0) and cooled down for 20 min at room temperature (RT). Sections were subsequently incubated overnight at 4ºC with primary antibodies, followed by incubation with fluorescently labeled secondary antibodies and DAPI in 0.2% Triton X-100, 1% horse serum, 1X PBS buffer for 45 min at RT. Sections were mounted with Vectashield mounting medium. Primary antibodies used were: Bhlhb5 1:200; Ctip2 1:2000; GFP 1:2000; Dbx1 1:10000; Delta1 1:100; Jag1 1:500; Ncad 1:400; Nurr1/Nr4A2 1:200; 1: Pax6 1:1000; Pcdh8 1:700; Pcdh19 1:500; pH3 1:500. Secondary antibodies used were: Alexa 488 1:700; Cy3 1:700; Cy5 1:500

cDNA synthesis and qPCR

RNA samples from electroporated tissue were retro-transcribed to cDNA using the RevertAid First First Strand cDNA Synthesis Ki, according to the supplier's instructions. For qPCR analysis of gene expression in each electroporated region we used 500 ng of RNA. The genomic DNA was removed by incubation for 30 min in 37ºC with DNase I, RNase-free. All qPCR reactions were performed on an Eppendorf machine in 20 µl reactio volume of Go Tag qPCR Master Mix (1× SYBR®Green PCR Master Mix and 200 nM of each primer). The following thermal program was applied: denaturation for 2 min at 95°C followed by 40 amplification cycles of 15 sec denaturing step (95°C) and 1 min annealing–extension step (60°C). Afterwards, to verify that results are coming from the single transcript the automatic program for melting curve analysis was performed using standard machine settings.

***In situ* hybridization**

In situ hybridization was performed as previously described (Griveau et al., 2010). For each gene of interest, a DNA fragment (typically 500-800 bp) was amplified by PCRs from an embryonic brain cDNA library using Phusion polymerase (Thermo) and primers indicated in Table 1. The promoter sequence of the T7 RNA polymerase (GGTAATACGACTCACTATAGGG) was added 5′ of the reverse primers. Antisense RNA probes were labeled using a DIG-RNA labeling kit (Roche). Alternatively, for mouse *Gsx2*, *Lhx2* (gift from Dr S. Retaux), *Notch1* (gift from Prof U. Lendahl) and *Shh* (gift from Dr S. Garel), a plasmid containing part of the cDNA was linearized by restriction enzyme digestion and subsequently submitted to reverse transcription. Sections were mounted with Mowiol 4-88.

Image acquisition and quantifications

In situ hybridization images were obtained using a Hamamatsu Nanozoomer 2.0 slide scanner (Hamamatsu Nanozoomer 2.0HT) with a 20X objective. The scans were verified using NDP Viewers and imported into Adobe Photoshop for figure adjustments.

All fluorescence images and tile scan images were acquired using a Leica TCS SP8 SMD confocal microscope equipped with a 40X objective, analyzed with ImageJ and imported into Adobe Photoshop for figure adjustments. Quantifications were performed by counting the proportion of GFP^+ cells among the selected marker positive population using the ImageJ software.

EdU pulse labeling and staining

EdU injection was carried out by intraperitoneal injection of 100 µL of 1 mg/ml EdU (Invitrogen) in PBS into pregnant females at E12.5 after electroporation at E11.5. Immunofluorescence and EdU staining was performed using Click iT EdU Alexa Fluor 647 Imaging Kit (Invitrogen).

Cell culture, transfection and sample preparation

Human embryonic kidney (HEK) 293T cells were grown in Dulbecco's modified Eagle's medium (DMEM; Gibco) containing 10% fetal bovine serum (FBS) and 1% penicillin-streptomycin (P/S; Gibco) and maintained at 37ºC in a 5% CO_2 atmosphere. Cells were seeded onto 6-multiwell plates at a density of 62500 cells/cm^2. Twenty-four hours later, transfection with 2 µg of pCAGGS constructs containing control GFP or Pcdh8, and with 4 µg of Pcdh8 scrambled shRNA or Pcdh8 shRNA was performed for 4h using Lipofectamine 2000 (Invitrogen) according to the manufacturer's instructions. Non-transfected cells (treated with transfection reagent only) were also used as control. Cells were maintained in serum-free Opti-MEM (Gibco) supplemented with 1% P/S after transfection and cultured for an additional 40h. Cell lysates were collected using RIPA buffer (50 mM Tris-HCl pH 7.5, 150 mM NaCl, 1% NP-40, 0.1% SDS, 0.5% sodium deoxycholate) supplemented with 2 mM EDTA and protease inhibitors (cOmplete™ EDTA-free tablets, Roche). Samples were then left in a rotator for 30 min at 4ºC to better dissolve the proteins and centrifuged at max speed for 10 min at 4ºC in order to pellet out crude undissolved fractions. The supernatant was stored at -20ºC until use. Protein quantification was determined using the bicinchoninic acid (BCA) protein assay reagent kit (Pierce™, ThermoFisher Scientific, USA) using bovine serum albumin (BSA) as standard.

Western blot analysis

Proteins samples were added to 1/4 volume of 4X LDS sample buffer (141 mM Tris, 106 mM Tris-HCl, 2% LDS, 10% glycerol, 0.51 mM EDTA, 0.22 mM SERVA Blue G, 0.175 mM phenol red, pH 8.5), to 1/10 of sample reducing agent 10X (50 mM DTT) and boiled at 95°C for 5 min. Protein samples (10 µg of lysates) were separated by SDS-PAGE on 3-8% tris-acetate gels (NuPAGE, Invitrogen) under reducing conditions at 150 V at 4ºC and electro-transferred to 0.45 µm nitrocellulose membranes for 1h30-2h at 0.5 A at 4ºC. After 1h blocking at RT with 5% (w/v) milk in Tris-buffered saline (50 mM Tris, 150 mM NaCl, pH 7.6) containing 0.1% Tween-20 (TBS-T), the membranes were incubated overnight at 4°C with the following primary antibodies: Pcdh8 1:1000, αTubulin 1:10000. After three washes of 10 min with TBS-T, the membranes were incubated with the appropriate HRP-conjugated secondary antibodies (1:20000) diluted in TBS-T with 5% (w/v) milk for 1h at RT. After three 10 min washes with TBS-T, blots were developed with SuperSignal West Pico Chemiluminescent Substrate (ThermoFisher Scientific) and visualized on the ChemiDoc apparatus (Bio-Rad). Densitometry analysis was determined using Image Lab™ software (Bio-Rad). The densities of protein bands were quantified with background subtraction. The bands were normalized to αTubulin loading control. The molecular weights were determined by using an appropriate pre-stained protein standard (HiMark 31-460 kDa, Invitrogen).

Microarray and scRNAseq analysis

Dbx1^{Cre};ROSA26^{YFP} cell sorting and microarray analysis at E12.5 were performed as previously described in (Griveau *et al.*, 2010). scRNAseq was performed as previously described for the VP (Moreau *et al.*, 2021). For the septum analysis, explants encompassing the septum were dissected from eight E11.5 *PGK^{Cre};Rosa26^{YFP}* embryos originating from two distinct litters and four E12.5 *Dbx1^{Cre};Rosa26^{tdTomato}* embryos from two litters. Explants were

pooled and dissociated using the Neural Tissue Dissociation Kit (P) (Miltenyi Biotec) and a gentleMACS Octo Dissociator following the manufacturer's instructions. Cell clumps and debris were removed via filtration through 30 µm cell strainers (Miltenyi Biotec) followed by two consecutive rounds of centrifugation for 3 min at 200 *g*. Pipetting through Gel Saver tips (QSP) and a final filtration using a 10 µm cell strainer (pluriSelect) allowed to obtain a single-cell suspension. Approximatively 10000 cells were used as input on the 10X Genomics Chromium controller. A Single Cell 3′ Kit v2 library was produced and sequenced on a NextSeq500 sequencer at a total depth of 476 million reads. Raw sequencing reads were processed to count matrix with Cell Ranger version 2.1.1 using default parameters and the mm10 mouse genome reference to which the sequenced of *YFP* and *tdTomato* were added. Bioinformatic analyses were performed with a R version 4.1.1. Cells were filtered based on the percentage of mitochondrial reads, removing those outside three median absolute deviation (MAD) from the median. The count matrix was library size normalized using Seurat V4.1.0 (Hao *et al.*, 2021). Doublet removal was achieved using Scrublet (Wolock *et al.*, 2019). Dimensionality reduction was achieved using the SPRING tool (Weinreb *et al.*, 2018).

Additional resources

A Shiny App to explore scRNAseq data from the mouse septum is available at: https://apps.institutimagine.org/mouse_septum/. Additionally, the Shiny App that allows making the pseudotime reconstructions of the ventral pallium (Moreau *et al.*, 2021) is available at: https://apps.institutimagine.org/mouse_pallium/.

Data and code availability

Raw scRNAseq reads and processed count matrix are available from GEO (Accession number GSE229603). The barcodes, SPRING coordinates and metadata of cells retained after quality control, as well as annotated R codes have been deposited at https://fcauseret.github.io/septum/.

Statistical Analysis

All data are expressed as mean ± SEM. *P*-values < 0.05 were considered significant and set as follows: **p*<0.05, ***p*<0.01, ****p*<0.001, *****p*<0.0001. According to the data structure, two-group comparisons were performed using two-tailed unpaired Student *t*-test or Holm-Sidak as *post-hoc* test following one- way ANOVA. Statistics and plotting were performed using GraphPad Prism 7.0 (GraphPad Software Inc, USA).

REFERENCES

Arai Y, Cwetsch AW, Coppola E, Shimogori T, Onofrio GD, Pierani A, et al. Evolutionary Gain of Dbx1 Expression Drives Subplate Identity in the Cerebral Cortex Article Evolutionary Gain of Dbx1 Expression Drives Subplate Identity in the Cerebral Cortex. CellReports 2019; 29: 645-658.e5.

Bassani S, Cwetsch AW, Gerosa L, Serratto GM, Folci A, Hall IF, et al. The female epilepsy protein PCDH19 is a new GABAAR-binding partner that regulates GABAergic transmission as well as migration and morphological maturation of hippocampal neurons. Hum Mol Genet 2018; 26: 1027–1038.

Bielle F, Griveau A, Narboux-Nême N, Vigneau S, Sigrist M, Arber S, et al. Multiple origins of Cajal-Retzius cells at the borders of the developing pallium. Nat Neurosci 2005; 8: 1002–1012.

Biswas S, Emond MR, Jontes JD. Protocadherin-19 and N-cadherin interact to control cell movements during anterior neurulation. J Cell Biol 2010; 191: 1029–1041.

Bouvier J, Thoby-Brisson M, Renier N, Dubreuil V, Ericson J, Champagnat J, et al. Hindbrain interneurons and axon guidance signaling critical for breathing. Nat Neurosci 2010; 13: 1066–1074.

Bruining H, Matsui A, Oguro-Ando A, Kahn RS, Van'T Spijker HM, Akkermans G, et al. Genetic mapping in mice reveals the involvement of Pcdh9 in long-term social and object recognition and sensorimotor development. Biol Psychiatry 2015; 78: 485–495.

Cooper SR, Emond MR, Duy PQ, Liebau BG, Wolman MA, Jontes JD. Protocadherins control the modular assembly of neuronal columns in the zebrafish optic tectum. J Cell Biol 2015; 211: 807–814.

Cwetsch AW, Ziogas I, Narducci R, Savardi A, Bolla M, Pinto B, et al. A rat model of a focal mosaic expression of PCDH19 replicates human brain developmental abnormalities and behaviours. Brain Commun 2022;

García-Moreno F, Anderton E, Jankowska M, Begbie J, Encinas JM, Irimia M, et al. Absence of Tangentially Migrating Glutamatergic Neurons in the Developing Avian Brain. Cell Rep 2018; 22: 96.

Godbole G, Roy A, Shetty AS, Tole S. Novel functions of LHX2 and PAX6 in the developing telencephalon revealed upon combined loss of both genes. Neural Dev 2017; 12: 1–8.

Griveau A, Borello U, Causeret F, Tissir F, Boggetto N, Karaz S, et al. A novel role for Dbx1-derived Cajal-Retzius cells in early regionalization of the cerebral cortical neuroepithelium. PLoS Biol 2010; 8

Halbleib JM, Nelson WJ. Cadherins in development: Cell adhesion, sorting, and tissue morphogenesis. Genes Dev 2006; 20: 3199–3214.

Hao Y, Hao S, Andersen-Nissen E, Mauck WM, Zheng S, Butler A, et al. Integrated analysis of multimodal single-cell data. Cell 2021; 184: 3573-3587.e29.

Kahr I, Vandepoele K, van Roy F. Delta-Protocadherins in Health and Disease. In: Progress in molecular biology and translational science. 2013. p. 169–192

Kong JH, Yang L, Dessaud E, Chuang K, Moore DM, Rohatgi R, et al. Notch Activity Modulates the Responsiveness of Neural Progenitors to Sonic Hedgehog Signaling. Dev Cell 2015; 33: 373.

Lasky JL, Wu H. Notch Signaling, Brain Development, and Human Disease. Pediatr Res 2005 577 2005; 57: 104–109.

Leung RF, George AM, Roussel EM, Faux MC, Wigle JT, Eisenstat DD. Genetic Regulation of Vertebrate Forebrain Development by Homeobox Genes. Front Neurosci 2022; 16: 1–35.

Lv X, Li S, Li J, Yu X-Y, Ge X, Li B, et al. Patterned cPCDH expression regulates the fine organization of the neocortex. Nat 2022 2022: 1–9.

Marklund U, Hansson EM, Sundström E, de Angelis MH, Przemeck GKH, Lendahl U, et al. Domain-specific control of neurogenesis achieved through patterned regulation of Notch ligand expression. Development 2010; 137: 437–445.

Moore R, Alexandre P. Delta-Notch Signaling: The Long and the Short of a Neuron's Influence on Progenitor Fates [Internet]. J Dev Biol 2020; 8[cited 2022 Dec 15] Available from: /pmc/articles/PMC7345741/

Moreau MX, Saillour Y, Cwetsch AW, Pierani A, Causeret F. Single-cell transcriptomics of the early developing mouse cerebral cortex disentangles the spatial and temporal components of neuronal fate acquisition. Development 2021

Pancho A, Aerts T, Mitsogiannis MD, Seuntjens E. Protocadherins at the Crossroad of Signaling Pathways. Front Mol Neurosci 2020; 13: 1–28.

Pataskar A, Jung J, Smialowski P, Noack F, Calegari F, Straub T, et al. NeuroD1 reprograms chromatin and transcription factor landscapes to induce the neuronal program. EMBO J 2016; 35: 24–45.

Peek SL, Mah KM, Weiner JA. Regulation of neural circuit formation by protocadherins. Cell Mol Life Sci 2017; 74: 4133–4157.

Pierani A, Brenner-Morton S, Chiang C, Jessell TM. A Sonic hedgehog-independent, retinoid-activated pathway of neurogenesis in the ventral spinal cord. Cell 1999; 97: 903–915.

Pierani A, Moran-Rivard L, Sunshine MJ, Littman DR, Goulding M, Jessell TM. Control of interneuron fate in the developing spinal cord by the progenitor homeodomain protein Dbx1. Neuron 2001; 29: 367–84.

Skaggs K, Martin DM, Novitch BG. Regulation of spinal interneuron development by the olig-related protein Bhlhb5 and notch signaling. Development 2011; 138: 3199–3211.

Sokolowski K, Tran T, Esumi S, Kamal Y, Oboti L, Lischinsky J, et al. Molecular and behavioral profiling of Dbx1-derived neurons in the arcuate, lateral and ventromedial hypothalamic nuclei. Neural Dev 2016; 11: 12.

Stump G, Durrer A, Klein AL, Lütolf S, Suter U, Taylor V. Notch1 and its ligands Delta-like and Jagged are expressed and active in distinct cell populations in the postnatal mouse brain. Mech Dev 2002; 114: 153–159.

Subramanian L, Sarkar A, Shetty AS, Muralidharan B, Padmanabhan H, Piper M, et al. Transcription factor Lhx2 is necessary and sufficient to suppress astrogliogenesis and promote neurogenesis in the developing hippocampus [Internet]. Proc Natl Acad Sci U S A 2011; 108[cited 2021 Aug 18] Available from: www.pnas.org/cgi/doi/10.1073/pnas.1101109108

Suzuki SC, Takeichi M. Cadherins in neuronal morphogenesis and function. Dev Growth Differ 2008

Szczurkowska J, Cwetsch AW, Dal Maschio M, Ghezzi D, Ratto GM, Cancedda L. Targeted in vivo genetic manipulation of the mouse or rat brain by in utero electroporation with a triple-electrode probe. Nat Protoc 2016; 11: 1552–1558.

Tokunaga A, Kohyama J, Yoshida T, Nakao K, Sawamoto K, Okano H. Mapping spatio-temporal activation of Notch signaling during neurogenesis and gliogenesis in the developing mouse brain. J Neurochem 2004; 90: 142–154.

Tsai T, Sikora M, Xia P, Colak-Champollion T, Knaut H, Heisenberg C-P, et al. An adhesion code ensures robust pattern formation during tissue morphogenesis. Science (80-) 2019; 116: 113–116.

Tsai TYC, Sikora M, Xia P, Colak-Champollion T, Knaut H, Heisenberg CP, et al. An adhesion code ensures robust pattern formation during tissue morphogenesis. Science 2020; 370: 113.

Wang H, Zang C, Liu XS, Aster JC. The Role of Notch Receptors in Transcriptional Regulation. J Cell Physiol 2015; 230: 982–988.

Ware M, Hamdi-Rozé H, Le Friec J, David V, Dupé V. Regulation of downstream neuronal genes by proneural transcription factors during initial neurogenesis in the vertebrate brain. Neural Dev 2016; 11: 1–15.

Weinreb C, Wolock S, Klein AM. SPRING: a kinetic interface for visualizing high dimensional single-cell expression data. Bioinformatics 2018; 34: 1246–1248.

Wolock SL, Lopez R, Klein AM. Scrublet: Computational Identification of Cell Doublets in Single-Cell Transcriptomic Data. Cell Syst 2019; 8: 281-291.e9.

Yang X, Tomita T, Wines-Samuelson M, Beglopoulos V, Tansey MG, Kopan R, et al. Notch1 Signaling Influences V2 Interneuron and Motor Neuron Development in the Spinal Cord. Dev Neurosci 2006; 28: 102–117.

Yasuda S, Tanaka H, Sugiura H, Okamura K, Sakaguchi T, Tran U, et al. Activity-Induced Protocadherin Arcadlin Regulates Dendritic Spine Number by Triggering N-Cadherin Endocytosis via TAO2β and p38 MAP Kinases. Neuron 2007; 56: 456–471.